

Faculty of Physics and Astronomy

University of Heidelberg



Diploma thesis
in Physics

submitted by
Sabine Schilling
born in Worms

September 2000

Implementation of BGF-processes in
Monte Carlo generators
for electron-proton scattering

This diploma thesis has been carried out by Sabine Schilling at the
Physical Institute
under the supervision of
Privatdozent Dr. Peter Schleper

Übersicht

Die korrekte Simulation von Prozessen höherer Ordnung ist von großer Bedeutung am Elektron-Proton Speicherring HERA. Das von J. Collins unlängst vorgestellte Regularisierungsschema, das eine konsistente Behandlung von Boson-Gluon-Prozessen der Ordnung $\alpha\alpha_s$ in einem Ereignis-Generator ermöglicht, wurde im Rahmen dieser Arbeit erstmals quantitativ untersucht. Es wurde gezeigt, dass dieses neue Schema sowohl zur Beschreibung tiefinelastischer Streuprozesse bei kleinem x -Björken als auch zur Beschreibung diffraktiver Ereignissen besonders geeignet ist. Beiden Prozessen ist gemein, dass die Gluondichte sehr viel größer als die Quarkdichten ist.

Abstract

The correct simulation of higher order processes is of big importance at the lepton-proton collider HERA. Recently a new regularization scheme was introduced by J. Collins, which allows a consistent treatment of the boson-gluon fusion process of order $\alpha\alpha_s$. This scheme is studied quantitatively for the first time in this thesis. It is demonstrated that the new scheme is especially important for the description of deep inelastic scattering at low x and for diffraction, where the gluon density is much larger than the quark densities.

Contents

1	Introduction	1
2	Deep inelastic scattering	3
2.1	Kinematics of electron–proton scattering	3
2.2	The naive parton model	4
2.3	Quantum Chromodynamics	5
2.3.1	QCD improved quark parton model	7
3	Next to leading order processes	9
3.1	General Kinematics	9
3.2	Boson – Gluon Fusion	10
3.2.1	Kinematics	10
3.2.2	The cross section for transverse polarized photons	11
3.2.3	The cross section for longitudinal polarized photons	13
3.2.4	Boson–Gluon–Fusion for the charm quark	14
3.2.5	Comparison with experimental results	15
3.3	QCD Compton Scattering	15
3.3.1	Kinematics	15
3.3.2	The cross section	16
3.4	The cut off scale p_T	18
4	QCD parton shower evolution	21
4.1	The Altarelli–Parisi evolution equation	21
4.2	QCD parton shower evolution	23
4.3	Kinematics of the off-shell struck quark	24
4.4	Bengtsson and Sjöstrand algorithm	25
4.5	Parton shower versus matrix elements	26
5	Subtraction method for Boson-Gluon-Fusion	29
5.1	The LO contribution	30
5.1.1	Basic Monte Carlo algorithm	30
5.1.2	First-order term	30
5.2	Boson-gluon fusion with subtraction	32
5.2.1	Computing of $F_2^{\text{BGF, hard}}$	35
5.2.2	Diffractive DIS	38
5.3	Comparison with $\overline{\text{MS}}$ scheme	39

6	Conclusion	47
A	Integration methods	49
A.1	Linear integration method	49
A.2	Importance sampling method	49
A.2.1	Example #1: $g(x) = \frac{1}{x}$	50
A.2.2	Example #2: $f(x) = \frac{a}{1+x} + \frac{b}{1-x}$	51
A.3	Calculation of F_2^{charm}	51
A.3.1	Results of the numeric integration	51
A.3.2	F_2^{charm} with the importance sampling method	53
B	Regularization of BGF in the Massive–Gluon scheme	55
	List of figures	59
	Acknowledgements	63
	Erklärung	65

Chapter 1

Introduction

Deep inelastic scattering (DIS) at HERA is the scattering of an electron with a quark of the proton. This scattering process can be described in the *Quark-Parton-model*(QPM). The higher the momentum transfer is, the better the structure of the proton can be resolved. The electron-proton accelerator HERA gives a worldwide unique possibility to investigate the structure of the proton. DIS is the leading order (LO) process in electron-proton collisions at HERA. Tests of the Standard Model (SM) require a description of the underlying physical processes with the highest possible accuracy. Therefore it is necessary to include higher order corrections to the leading order process. These higher order corrections are calculated in Quantum Chromodynamics (QCD), the theory of strong interactions. The next to leading order (NLO) corrections are the QCD-Compton process, where an additional gluon is radiated from the struck quark, the boson-gluon fusion (BGF) process, where the photon interacts with the gluon by an intermediate quark and the virtual (loop) corrections. The matrix elements for these processes diverge individually, however regularization schemes can be applied to obtain finite results. The NLO corrections are derived by a perturbative expansion of the LO contribution. Whereas in Quantum Electrodynamics the perturbation series converges relatively fast due to the small value of the expansion parameter α_{em} , this is not the case for QCD processes, as large α_s (corresponding to small Q^2) values make the perturbative series only slowly convergent. For large values of α_s the emission rate is increasing as one approaches the non-perturbative regime, the NLO contributions, which should be only correction to the LO contribution, become larger than the LO contribution.

Another approach to reach higher accuracy is given by parton showers (PS's). By a resummation of large logarithmic terms in Q^2 it is possible to get a reasonable description also in regions in which α_s assumes large values ([1]). The weak point of the PS description is the treatment of wide-angle parton emission. In this region many Feynman diagrams may contribute with comparable strengths, thus the final cross section may depend on the detailed interference effects between these diagrams which are not present in PS description.

Neither PS nor perturbation series alone are able to describe the physics in the whole phase space and it would be ideal to include both descriptions in an event generator. In [2] Collins describes how it is possible to implement consistently NLO corrections in an event generator. An important question is the matching between both contributions,

he solves this problem by a so called *subtraction method* and displays the mandatory calculations explicitly for the order α_s corrections due to Boson–Gluon Fusion (BGF) processes. One important application of this method will be diffractive physics, as a gluon dominated object would lead to a dominating contribution of BGF processes to the cross section, the NLO correction would not be anymore a small contribution to the total cross section.

In this thesis the theoretical description of the subtraction method has been applied for the first time and the numerical techniques for evaluating the NLO contribution due to BGF processes have been developed. This new regularization scheme could thus be applied to inclusive DIS as well as diffractive DIS at HERA. The outline of this thesis is as follows: after an introduction to deep inelastic scattering the NLO corrections to this process are discussed in chapter 3. In chapter 4 the basic concepts of parton shower evolution in the Altarelli-Parisi approximation are summarized. In chapter 5 we will then explain the subtraction method and display the obtained numerical results. A detailed discussion of the necessary integration methods is given in appendix A while in appendix B we show the regularization of BGF processes in the Massive Gluon scheme, a standard regularization scheme.

Chapter 2

Deep inelastic scattering

2.1 Kinematics of electron–proton scattering

The standard model describes the scattering of an electron e on a proton p by the exchange of virtual gauge bosons, i.e. photons for the electromagnetic interaction, Z^0 and W^\pm for the electroweak interaction. Because of the high masses of the electro-weak gauge bosons Z^0 and W^\pm , the photon exchange gives the dominant contribution to the cross section at the center of mass energy of 320 GeV available at HERA¹. In order to

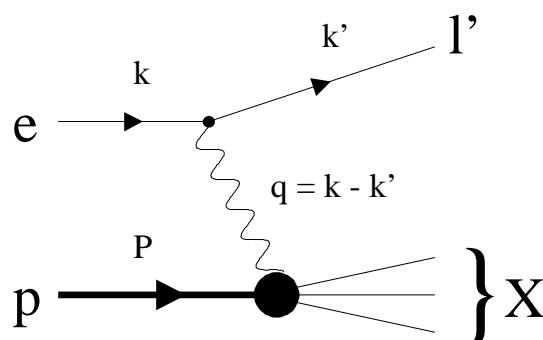


Figure 2.1: e - p -scattering.

describe the kinematics of $e - p$ scattering we introduce the definitions for the relevant four vectors (E, \vec{p}) of the scattering process:

- k : incoming electron e
- k' : outgoing lepton l'
- P : incoming proton p

The exchanged four momentum $q = (\nu, \vec{q})$ is given by

$$q = k - k' = P_X - P, \tag{2.1}$$

where P_X is the sum of the four momenta of all particles in the hadronic final state.

¹HERA is the electron proton collider at DESY (Hamburg).

Furthermore we can define the following (frame independent) Lorentz scalars :

$$Q^2 \equiv -q^2, \quad (2.2)$$

$$s \equiv (k + P)^2 \approx 4E_e E_p, \quad (2.3)$$

$$y \equiv \frac{P \cdot q}{P \cdot k}, \quad (2.4)$$

$$x \equiv \frac{Q^2}{2P \cdot q} = \frac{Q^2}{y \cdot s}, \quad (2.5)$$

where s is the square of the total center of mass energy, and y and x are the *Bjorken scaling variables*. These dimensionless variables measure momentum fractions: The fraction of the electron momentum carried by the photon is given by y , while x corresponds to the fraction of the proton momentum carried by the struck parton inside the proton. X includes all particles except the scattered lepton. The hadronic final state is given by W :

$$W^2 = (q + P)^2 \approx -Q^2 + ys = Q^2 \frac{1-x}{1}. \quad (2.6)$$

The \approx indicates that the masses of the electron and the proton are negligible compared to s .

The variables x , y and Q^2 are not independent of each other, but connected by the square of the center of mass energy s :

$$Q^2 = sxy. \quad (2.7)$$

Using the above notation we can now define the kinematical requirements for inelastic lepton nucleon scattering. Inelastic lepton nucleon scattering $ep \rightarrow e'X$ is characterized by $W^2 \gg m_p^2$, where m_p is the proton mass, deep inelastic scattering *DIS* is defined by the additional requirement $Q^2 \gg m_p^2$.

2.2 The naive parton model

In the naive parton model the constituents of the proton, the quarks, do not interact with each other.

In this model *DIS* is described as the *incoherent sum of elastic scattering of the electrons on the quasifree constituents of the proton*[3]. The basic cross section, before any QCD radiation is taken into account, may generically be written as

$$d\sigma = (\text{boson propagator}) \times (\text{parton distributions}) \\ \times (\text{lepton - boson - parton couplings}) \times (\text{helicity factors}). \quad (2.8)$$

In DIS the quark masses can be neglected, if the following relations hold:

$$-q^2 = Q^2 \gg p_1^2 \quad \text{and} \quad Q^2 \gg p_1'^2, \quad (2.9)$$

where q is the four momentum of the incoming photon, p_1 the four momentum of the incoming quark and p_1' the four momentum of the outgoing quark.

Applying the Feynman rules we can calculate the double differential cross section for elastic electron-proton scattering (see [4])

$$\frac{d^2\sigma}{dx dQ^2} = \frac{4\pi\alpha_{em}^2}{Q^4 x} \left(\frac{y^2}{2} + 1 - y \right) F_2(x), \quad (2.10)$$

where the contributions of the different quarks and antiquarks are summarized in the structure function $F_2(x)$

$$F_2(x) = x \sum_a e_a^2 f_a(x). \quad (2.11)$$

$f_a(x)$ is the density of quarks of flavour a in the proton as a function of the carried fraction of momentum and e_a the corresponding electric charge. The sum in eq. (2.11) runs over quark and antiquark flavours².

For later usage we will rewrite eq. (3.1) as a double differential cross section of x and y . With $Q^2 = xys$ it follows:

$$\frac{d^2\sigma}{dx dy} = K F_2(x), \quad (2.12)$$

where

$$K = \frac{4\pi\alpha^2}{s x^2 y^2} \left(\frac{y^2}{2} + 1 - y \right) \quad (2.13)$$

and y defined in eq. (2.4).

Eq. (2.12) can also be written as function of y and Q^2 :

$$\frac{d^2\sigma}{dy dQ^2} = \frac{4\pi\alpha^2}{Q^2 y} \left(\frac{y^2}{2} + 1 - y \right) F_2(x). \quad (2.14)$$

2.3 Quantum Chromodynamics

In the naive quark parton model (QPM) the process of electron proton scattering is described by the Born term ($\gamma^* q \rightarrow q$). The naive parton model completely ignores the dynamical role of gluons as carriers of the strong interaction associated with coloured quarks, which is described by Quantum Chromodynamics (QCD). The essential properties of QCD are [4]:

- besides their electric charge quarks carry an additional quantum number called “colour”; there are three colours R (Red), G (Green) and B (Blue);
- colour is exchanged by eight bicoloured gluons;
- as gluons themselves carry colour charge they can interact with quarks *and* other gluons;

²Eq. (3.1) is the differential cross section given by the exchange of a virtual photon and corresponds to the dominant contribution to the Neutral Current (NC) processes. The full structure of the NC includes interference terms between the neutral gauge bosons γ and Z^0 and is rather complicated. Furthermore it does not take into account effects introduced by polarization of initial state.

- the running coupling constant of QCD in first order of QCD perturbation theory is a function of the transferred four momentum Q^2 and is given by

$$\alpha_s(Q^2) = \frac{12\pi}{(33 - 2n_f) \log(\frac{Q^2}{\Lambda^2})}, \quad (2.15)$$

where n_f is the number of active quark flavours at Q^2 and Λ is the QCD mass scale. The value of Λ is not predicted by the theory, it is a free parameter to be determined from experiment. Its value is in the range of 0.1 to 0.5 GeV.

In order to use QCD perturbation theory, α_s must be significantly smaller than 1, such that the perturbation series converges rapidly with any higher order correction. Given e.g. $Q^2 = 900 \text{ GeV}^2$, then α_s is of order 0.1 and QCD perturbation theory can be applied. As α_s decreases with increasing Q^2 , we say that the theory is *asymptotically free*, therefore, probing the structure of the nucleon at high values of Q^2 quarks and gluons behave as free, non interacting particles. On the other hand α_s becomes very big for small Q^2 : free coloured particles can not exist anymore, but they are combined colour neutral hadrons (*confinement*).

- Quark-gluon interactions are computed using the rules of QED with the substitution $\sqrt{\alpha} \rightarrow \sqrt{\alpha_s}$ at each vertex.

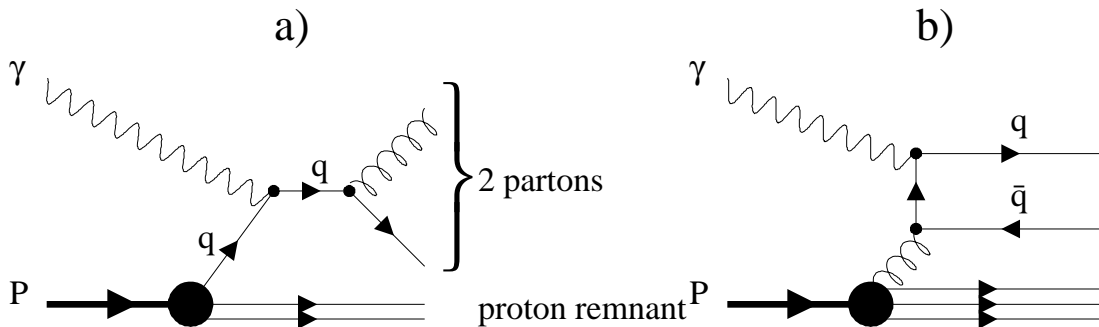


Figure 2.2: Parton processes in leading order QCD:

(a) QCD-Compton-scattering,

(b) Boson-Gluon-Fusion (the crossed diagrams are in both cases not shown).

The naive parton model ignores the fact that partons (quarks *and* gluons) can radiate gluons. Fig (2.2) shows the corrections in leading order QCD (order α_s) to the Born term $\gamma q \rightarrow q'$: a gluon constituent of the target can contribute to deep inelastic scattering through $(\gamma^* g \rightarrow q\bar{q})$ pair production. This process is called *Boson-Gluon Fusion* (BGF).

Moreover, a gluon can be emitted before or after the scattering of the photon on a quark ($\gamma^* q \rightarrow qg$), the so called *QCD-Compton* scattering (QCDC).

In order to calculate the full order α_s ($\mathcal{O}(\alpha_s)$) corrections to the quark model we finally have to take into account the *virtual corrections*: a gluon can be emitted before or after the scattering of the photon on the quark and be absorbed by the same quark, furthermore, a gluon can be emitted by the incoming quark and be absorbed by the outgoing quark (see eq. (2.16)).

The contributions of the $\mathcal{O}(\alpha_s)$ corrections (QCDC, BGF and the virtual corrections) to the structure function can be written as

$$\begin{aligned}
F_2 &= \left| \begin{array}{c} \text{Born term} \\ + \text{BGF} \\ + \text{QCDC} \end{array} \right|^2 \\
&+ \left| \begin{array}{c} \text{virtual corrections} \\ + \text{BGF} \\ + \text{QCDC} \end{array} \right|^2 + \mathcal{O}(\alpha_s^2) \\
&= \left| F_2^{\text{QPM}} + \text{virtual corrections} \right|^2 + \left| F_2^{\text{BGF}} + F_2^{\text{QCDC}} \right|^2 + \mathcal{O}(\alpha_s^2).
\end{aligned} \tag{2.16}$$

Whereas the Born term is of order α (and zeroth order α_s) all other terms are of $\mathcal{O}(\alpha\alpha_s)$ ($\mathcal{O}(\alpha\alpha_s)$ will be abbreviated as $\mathcal{O}(\alpha_s)$ in the following sections). The contributions from BGF and QCDC will be discussed more in detail in the following chapter.

2.3.1 QCD improved quark parton model

Whereas in the naive parton model quarks do not interact with each other, in QCD they interact through the exchange of gluons. The $\mathcal{O}(\alpha_s)$ corrections to the Born term lead to a Q^2 dependence of the structure function $F_2(x, Q^2)$. In the naive parton model with quarks of spin $\frac{1}{2}$ and no gluons the nucleon structure functions F_1 and F_2 are related by the Callan-Cross relation

$$F_2 = 2xF_1. \tag{2.17}$$

If we consider the existence of gluons, the Callan-Cross relation eq. (2.17) does not hold anymore and has to be replaced by

$$F_L(x, Q^2) = F_2(x, Q^2) - 2xF_1(x, Q^2), \tag{2.18}$$

where F_L is the longitudinal structure function. Neglecting the proton and electron mass the spin averaged double differential cross section for deep inelastic scattering can be written as the product of the two nucleon structure functions $F_1(x, Q^2)$ and $F_2(x, Q^2)$, with the flux of virtual photons coming from the electron [4]

$$\frac{d\sigma(ep \rightarrow e'X)}{dy dQ^2} = \frac{4\pi\alpha^2}{yQ^4} \left((1-y) F_2(x, Q^2) + y^2 x F_1(x, Q^2) \right). \tag{2.19}$$

With eq.(2.18), eq.(2.19) can be rewritten in terms of the structure functions F_2 and F_L

$$\frac{d\sigma(ep \rightarrow e'X)}{dy dQ^2} = \frac{4\pi\alpha^2}{yQ^4} \left(\left(1 - y + \frac{y^2}{2} \right) F_2(x, Q^2) - \frac{y^2}{2} F_L(x, Q^2) \right). \tag{2.20}$$

For all $e - p$ processes the flux of photons can be factorised, so that the cross section is given as a product of the flux of virtual photons with the γ^*p cross section:

$$\frac{d\sigma(ep \rightarrow e'X)}{dydQ^2} = \Gamma(y, Q^2) [\sigma_T(\gamma^*p \rightarrow X) + \epsilon\sigma_L(\gamma^*p \rightarrow X)] \quad (2.21)$$

where $\Gamma(y, Q^2)$ represents the flux of virtual photons from the electron

$$\Gamma(y, Q^2) = \frac{\alpha}{yQ^2\pi} \left(\left(1 - y + \frac{y^2}{2} \right) - \frac{m_e^2 y^2}{Q^2} \right) \quad (2.22)$$

and ϵ is the ratio of the flux of longitudinal and transverse photons

$$\epsilon = \frac{1 - y}{1 - y + \frac{y^2}{2}}. \quad (2.23)$$

The cross section for transverse and longitudinal virtual photons is given by:

$$\sigma_T(\gamma^*p \rightarrow X) = \frac{4\pi^2\alpha}{Q^2} 2xF_1(x, Q^2) = \frac{4\pi^2\alpha}{Q^2} (F_2(x, Q^2) - F_L(x, Q^2)); \quad (2.24)$$

$$\sigma_L(\gamma^*p \rightarrow X) = \frac{4\pi^2\alpha}{Q^2} (F_2(x, Q^2) - 2xF_1(x, Q^2)) = \frac{4\pi^2\alpha}{Q^2} F_L(x, Q^2). \quad (2.25)$$

Adding of eqs. (2.24) and (2.25), we can correlate the cross sections of longitudinal and transverse polarized photons with the proton structure function F_2 :

$$F_2(x, Q^2) = \frac{Q^2}{4\pi^2\alpha} (\sigma_T(\gamma^*p \rightarrow X) + \sigma_L(\gamma^*p \rightarrow X)). \quad (2.26)$$

Chapter 3

Next to leading order processes

The matrix elements of Boson Gluon Fusion (BGF) and QCD Compton scattering (QCDC) are derived in first order QCD perturbation theory. The contributions of this next-to-leading (NLO) corrections to the leading order Born Term will be derived in this chapter.

For both processes we will give first a short overview of the underlying kinematics and then display separately the matrix elements for transverse and longitudinal polarized photons, from which we derive the cross sections. Problematic is hereby that the matrix elements for transverse polarized photons of BGF and QCDC show divergences in the collinear region. We are therefore forced to introduce a cut parameter to obtain a finite cross section due to transverse polarized photons. As cut parameter we will chose a minimal transverse momentum of the outgoing quark, p_T^{min} .

3.1 General Kinematics

The contribution of the $\mathcal{O}(\alpha_s)$ corrections introduced by BGF and QCD-Compton processes to the differential cross section of the light quarks has been calculated by Peccei and Rückl in [5].

They define an additional scaling variable¹

$$c_i = \frac{P \cdot p_i}{P \cdot q}, \quad (3.1)$$

where p_i is the four-momentum of an outgoing quark, q is the four-momentum of the incoming photon and P is the four-momentum of the proton. In the proton rest frame we have $P = (M_P; 0, 0, 0)$, where M_P is the mass of the proton. With the four-momentum of the outgoing quark given by $p_i = (E_i, p_{i1}, p_{i2}, p_{i3})$ c_i becomes

$$c_i = \frac{E_i}{E_q}. \quad (3.2)$$

In the rest frame of the proton c_i is the fraction of the photon energy that is carried by the outgoing particle. Given ξ as the momentum fraction of the struck parton (a

¹In [5] this variable is called z_i .

gluon in the case of BGF resp. a quark for QCD) we can define the variable

$$z = \frac{x}{\xi}. \quad (3.3)$$

The meaning of the scaling variable z can be illustrated by the following example (see fig. (3.1)) suppose there is a branching of the parton a into two partons b and c . If

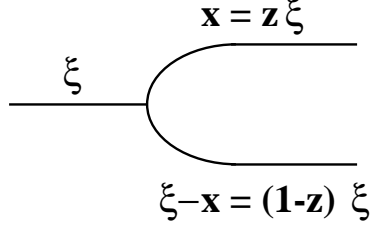


Figure 3.1: *Splitting of a parton with momentum ξ into two partons with momentum fraction z and $(1 - z)$ respectively.*

parton a carries momentum ξ and parton b carries a fraction z of the momentum of a , then the momentum of parton b is $x = z\xi$. Momentum conservation requires then that parton c carries a momentum $\xi - x = (1 - z)\xi$.

3.2 Boson – Gluon Fusion

3.2.1 Kinematics

The Lorentz invariant *Mandelstam variables* are conventionally used to express the invariant amplitude \mathcal{M} of a two body scattering process $A B \rightarrow C D$:

$$\begin{aligned} s &= (p_A + p_B)^2 = (p_C + p_D)^2, \\ t &= (p_A - p_C)^2 = (p_B - p_D)^2, \\ u &= (p_A - p_D)^2 = (p_B - p_C)^2, \end{aligned} \quad (3.4)$$

where p_A, p_B, p_C and p_D are the four-momenta of the particles A, B, C and D .

In order to describe the kinematics of the process $\gamma^* g \rightarrow q\bar{q}$ (BGF) it is convenient to work in the γ^* -gluon center-of-mass frame. Neglecting the quark masses the Mandelstam variables for the process displayed in fig. (3.2) are given by

$$\begin{aligned} \hat{s} &= (q + g)^2 = (p_1 + p_2)^2 = -Q^2 + 2qg, \\ \hat{t} &= (q - p_1)^2 = (g - p_2)^2 = -2gp_2, \\ \hat{u} &= (q - p_2)^2 = (g - p_1)^2 = -2gp_1, \end{aligned} \quad (3.5)$$

where $g = \xi P$ is the four momentum of the incoming gluon, q is the four momentum of the incoming photon and p_1 and p_2 are the four momenta of the outgoing quarks. (3.2(b)):

$$\begin{aligned} \hat{s} &= (q + g)^2 = (p_2 + p_1)^2 = -Q^2 + 2qg, \\ \hat{t} &= (q - p_2)^2 = (g - p_1)^2 = -2gp_1, \\ \hat{u} &= (q - p_1)^2 = (g - p_2)^2 = -2gp_2. \end{aligned} \quad (3.6)$$

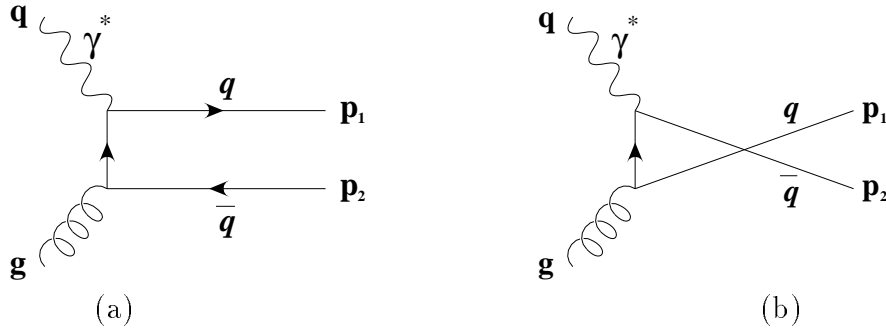


Figure 3.2: *Boson – Gluon Fusion:*

- (a) *momentum exchange between virtual photon and gluon in the t-channel,*
 (b) *BGF diagram with momentum exchange in the u-channel.*

The invariant variables are denoted $\hat{s}, \hat{t}, \hat{u}$ to indicate that we are considering a partonic subprocess. From eq. (3.5) and eq. (3.6) we see that the momentum transfer between the incoming gluon and photon is for the diagram (a) of fig.(3.2) in the t -channel, while for the crossed diagram (b) the momentum transfer is in the u -channel.

From eq. (3.5) follows that the Mandelstam are related by

$$\hat{s} + \hat{t} + \hat{u} = q^2 = -Q^2. \quad (3.7)$$

For the scaling variable z we obtain

$$z = \frac{x}{\xi} = \frac{Q^2}{2gq} = \frac{Q^2}{\hat{s} + Q^2}. \quad (3.8)$$

3.2.2 The cross section for transverse polarized photons

According to [5] we will display the results by giving separately the contribution of transverse and longitudinal polarized photons to the BGF cross section. The amplitude for transverse polarized photons is given by

$$|\mathcal{M}_T|^2 = 32 \frac{4}{8} \pi^2 e_q^2 \alpha \alpha_s \left(\frac{\hat{u}}{\hat{t}} + \frac{\hat{t}}{\hat{u}} - 2 \frac{\hat{s}Q^2}{\hat{u}\hat{t}} + \frac{4\hat{s}Q^2}{(\hat{s} + Q^2)^2} \right), \quad (3.9)$$

where $4/8$ is the colour factor and the sum over the polarisation states of the incoming virtual photon has been already performed. Eq. (3.9) can be derived by evaluating the corresponding QED process $\gamma^* e \rightarrow \gamma e$ using the Feynman rules of QED, substituting α^2 by $e_q^2 \alpha \alpha_s$ and exchanging u and t because of the different ordering of the outgoing particles. In eq. (3.9) the term \hat{u}/\hat{t} corresponds to the contribution of diagram (a) in fig. (3.2), and the term \hat{t}/\hat{u} to the contribution of the crossed diagram (b). The term $(-2\frac{\hat{s}Q^2}{\hat{u}\hat{t}})$ is the interference term between both diagrams. A two body cross section is generally given by [6]

$$\frac{d\sigma}{dt} = \frac{1}{64\pi} \frac{1}{s} \bar{p}_{1cm}^2 |\mathcal{M}|^2, \quad (3.10)$$

where

$$\vec{p}_{1cm}^2 = \frac{(p_1 p_2)^2 - m_1 m_2}{s} \quad (3.11)$$

is the momentum in the center of mass frame of particles 1 and 2. This formula can easily be applied to the partonic cross section. For BGF the following relations hold: $p_1 = q$ and $p_2 = g$. If we consider the incoming parton as massless, then eq. (3.11) becomes

$$\vec{p}_{1cm}^2 = \frac{(q g)^2}{\hat{s}} = \frac{(\hat{s} + Q^2)^2}{4\hat{s}}, \quad (3.12)$$

Then we get for differential cross section of transverse polarized photons

$$(3.13)$$

where we have used eq. (3.8). Now we want to express eq. (3.13) in terms of the scaling variable c_i : From eq. (3.5) we have

$$\begin{aligned} \hat{u} &= -2\xi P p_1 \\ \hat{t} &= -2\xi P p_2 \\ \hat{s} + Q^2 &= 2q\xi P, \end{aligned} \quad (3.14)$$

where ξ is the fraction of the proton momentum carried by the gluon.

Inserting eqs. (3.14) in eq. (3.1) leads then to

$$c_q \equiv c_{p_1} = \frac{P p_1}{P q} = -\frac{\hat{u}}{(\hat{s} + Q^2)} \quad (3.15)$$

$$c_2 \equiv c_{\bar{q}} = \frac{P p_2}{P q} = -\frac{\hat{t}}{(\hat{s} + Q^2)}. \quad (3.16)$$

With eq. (3.7) we derive the relation between c_q and $c_{\bar{q}}$

$$1 - c_q = c_{\bar{q}}, \quad (3.17)$$

as expected by energy-momentum conservation. From eq. (3.5) it follows that

$$\frac{d\hat{t}}{dc_q} = \hat{s} + Q^2 \quad (3.18)$$

and thus

$$\frac{d\hat{\sigma}_T}{dc_q} = \frac{1}{16\pi} \frac{1}{\hat{s} + Q^2} |\mathcal{M}_T|^2. \quad (3.19)$$

Using eq. (3.15) we can express the dependence of the amplitude on the Mandelstam variables in terms of the new scaling variables c_q and z :

$$\left(\frac{\hat{u}}{\hat{t}} + \frac{\hat{t}}{\hat{u}} - 2 \frac{\hat{s} Q^2}{\hat{u} \hat{t}} + \frac{4\hat{s} Q^2}{(\hat{s} + Q^2)^2} \right) = \frac{(c_q^2 + (1 - c_q)^2)(z^2 + (1 - z^2))}{(1 - c_q)c_q} \quad (3.20)$$

From eq. (3.20) we see that the cross section diverges for $c_q \rightarrow 0$ and $c_q \rightarrow 1$, therefore we are forced to introduce a cut parameter in order to integrate eq. (3.19). This last will can be the transverse momentum of the outgoing quark

$$p_T = |\vec{p}_1| \sin\theta, \quad (3.21)$$

where θ is the angle between the incoming photon and the outgoing quark with four momentum $p_1 = (E_1, \vec{p}_1)$. Making use of eq. (3.5) and eq. (3.3) p_T can be expressed in terms of the Mandelstam variables or c_q :

$$p_T^2 = \frac{\hat{s}\hat{t}\hat{u}}{(\hat{s} + Q^2)} = c_q(1 - c_q)\hat{s}. \quad (3.22)$$

Solving this equation for c_q we find the relation between the p_T cut parameter $p_{T, min}$ and the integration boundaries $c_{q, min}$ and $c_{q, max}$

$$\begin{aligned} c_{q, min} &= \frac{1 - \beta}{2} \\ c_{q, max} &= \frac{1 + \beta}{2} = 1 - c_{q, min} \end{aligned} \quad (3.23)$$

with

$$\beta = \sqrt{1 - \frac{4p_{T, min}^2}{\hat{s}}}. \quad (3.24)$$

With these conditions we can now integrate eq. (3.19) in order to obtain the cross section for transverse photons $\hat{\sigma}_T$

$$\begin{aligned} \hat{\sigma}_T &= \pi e_q^2 \alpha_s \frac{z}{Q^2} (z^2 + (1 - z^2)) \int_{c_{q, min}}^{c_{q, max}} \frac{c_q^2 + (1 - c_q)^2}{(1 - c_q)c_q} dc_q \\ &= 2\pi e_q^2 \alpha_s \frac{z}{Q^2} (z^2 + (1 - z)^2) \log\left(\frac{1 - c_{q, min}}{c_{q, min}}\right) - 2 + 4c_{q, min} \end{aligned} \quad (3.25)$$

Using eq. (3.23), the cross section for transversal photons eq. (3.25) can be expressed in terms of β :

$$\hat{\sigma}_T = 2\pi e_q^2 \alpha_s \frac{z}{Q^2} (z^2 + (1 - z)^2) \left(\log\frac{1 + \beta}{1 - \beta} - \beta\right). \quad (3.26)$$

3.2.3 The cross section for longitudinal polarized photons

According to [7] we find for the amplitude of the longitudinal photons

$$|\mathcal{M}_L|^2 = 16\pi^2 e_q^2 \alpha_s 8z(1 - z). \quad (3.27)$$

With eq. 3.13 we find then

$$\frac{d\hat{\sigma}_L}{d\hat{t}} = \pi e_q^2 \alpha_s \frac{z^2}{Q^4} 8z(1 - z). \quad (3.28)$$

This cross section does not diverge for $\hat{t} \rightarrow 0$, so the integration could be performed over the whole kinematic region. But as we have introduced a minimal p_T cut in the case of the transverse polarized photons we will use the same cut in this case: Using eq. 3.19 we obtain

$$\hat{\sigma}_L = \pi e_q^2 \alpha_s \frac{z}{Q^2} 8z(1 - z) \int_{c_{q, min}}^{c_{q, max}} dc_q \quad (3.29)$$

$$= \pi e_q^2 \alpha_s \frac{z}{Q^2} 8z(1 - z)\beta. \quad (3.30)$$

The total contribution of BGF processes to the cross section for light quarks is then obtained by multiplying the sum of eqs. (3.29) and (3.26) with the gluon density $f_g(\xi)$ and integrating over ξ

$$\sigma_{BGF} = \int_{ax}^1 (\hat{\sigma}_L + \hat{\sigma}_T) f_g(\xi) d\xi \quad (3.31)$$

where

$$a = 1 + \frac{4p_T^2 \min}{Q^2}. \quad (3.32)$$

Beyond the naive QPM the structure function becomes dependent on Q^2 . In general the structure function $F_2^p(x, Q^2)$ is related to the total cross section by eq. (2.26). Thus we get for

$$F_2^{\text{light, BGF}}(x, Q^2) = \sigma_{BGF} \frac{Q^2}{4\pi^2 \alpha}. \quad (3.33)$$

With eq. (3.33) we can now display the contribution of BGF processes to F_2 :

$$F_2^{\text{light BGF}}(x, Q^2, p_{T \min}) = \frac{1}{2\pi} e_q^2 \alpha_s(\mu^2) \int_{ax}^1 z C_{\text{light}} f_g(\xi, \mu^2) d\xi, \quad (3.34)$$

where

$$\mu^2 = Q^2$$

and

$$C_{\text{light}} = \left[(z^2 + (1-z)^2) \log \frac{1+\beta}{1-\beta} + \beta(-1 + 6z(1-z)) \right]. \quad (3.35)$$

3.2.4 Boson–Gluon–Fusion for the charm quark

In the previous section we calculated the structure function for light quarks eq. (3.34). Now we want to compare this result with the structure functions for charm quarks. In contrast to the light quarks, the mass of the charm quark can not be neglected. The contribution due to BGF processes to the structure function for the charm quarks is given by [8]:

$$F_2^{\text{charm, BGF}}(x, Q^2, m_c^2) = \frac{1}{2\pi} e_q^2 \alpha_s(\mu^2) \int_{ax}^1 C^{\text{charm}} z f_g(\xi, \mu^2) d\xi, \quad (3.36)$$

where:

$$a = 1 + \frac{4m_c^2}{Q^2}, \quad \mu^2 = (2m_c)^2, \quad \beta = \sqrt{1 - \frac{4m_c^2}{\hat{s}}}, \quad (3.37)$$

and

$$C^{\text{charm}} = \left[(z^2 + (1-z)^2 + z(1-3z)) \frac{4m_c^2}{Q^2} - z^2 \frac{8m_c^4}{Q^4} \right. \\ \left. \log \frac{1+\beta}{1-\beta} + \beta \left(-1 + 8z(1-z) - z(1-z) \frac{4m_c^2}{Q^2} \right) \right]. \quad (3.38)$$

In the computation of the structure function for light quarks, eq. (3.35), it was necessary to introduce a cut parameter p_T in order to avoid divergences. For charm quarks the charm mass m_c leads to a finite result for all values of p_T (see eq.(3.37)).

Due to the dependence on the gluon density the calculation of the integrals in eqs. (3.36) and (3.34) have to be performed numerically². (Details about the problems arising by the numerical integration of eqs. (3.36) and (3.34) are discussed in appendix A.3).

3.2.5 Comparison with experimental results

In this section we want to compare $F_2^{\text{charm, BGF}}$ calculated by numerical integration of eq. (3.36) with the measured values of the ZEUS collaboration published in [10] (see fig. (3.2.5)). In fig. (3.2.5) the data points show the measured values of F_2^{charm} , the curve is the calculated $F_2^{\text{charm BGF}}$. We observe a good agreement between the measured values and eq. (3.36) for all pairs of measured x and Q^2 values.

3.3 QCD Compton Scattering

3.3.1 Kinematics

In the QCD Compton scattering process $\gamma^*q \rightarrow qg$ a gluon can be emitted from the incoming quark (see fig. (3.4),(a)) or from the outgoing quark (fig. (3.4),(b)).

In the first case the Mandelstam variables are given by

$$\begin{aligned}\hat{s} &= (p_2 + g)^2 = (q + p_1)^2 = -Q^2 + 2qp_1, \\ \hat{t} &= (q - p_2)^2 = (p_1 - g)^2 = -2p_1g, \\ \hat{u} &= (p_1 - p_2)^2 = (q - g)^2 = -2qg,\end{aligned}\tag{3.39}$$

while in the second case by

$$\begin{aligned}\hat{s} &= (q + p_1)^2 = -Q^2 + 2qp_1, \\ \hat{t} &= (q - g)^2 = -2qg, \\ \hat{u} &= (p_1 - g)^2 = -2p_1g.\end{aligned}\tag{3.40}$$

The Mandelstam variables corresponding to fig. (3.4,(b)) are obtained by exchanging the values \hat{t} and \hat{u} corresponding fig. (3.4,(a)).

From eq. (3.39) we obtain:

$$\begin{aligned}\hat{s} + Q^2q &= \xi P, \\ \hat{t} &= -2\xi P g, \\ \hat{u} &= -2\xi q P.\end{aligned}\tag{3.41}$$

From eq. (3.1) follows then

²We used the integration routine *GADAP* from [9] to integrate eq. (3.36).

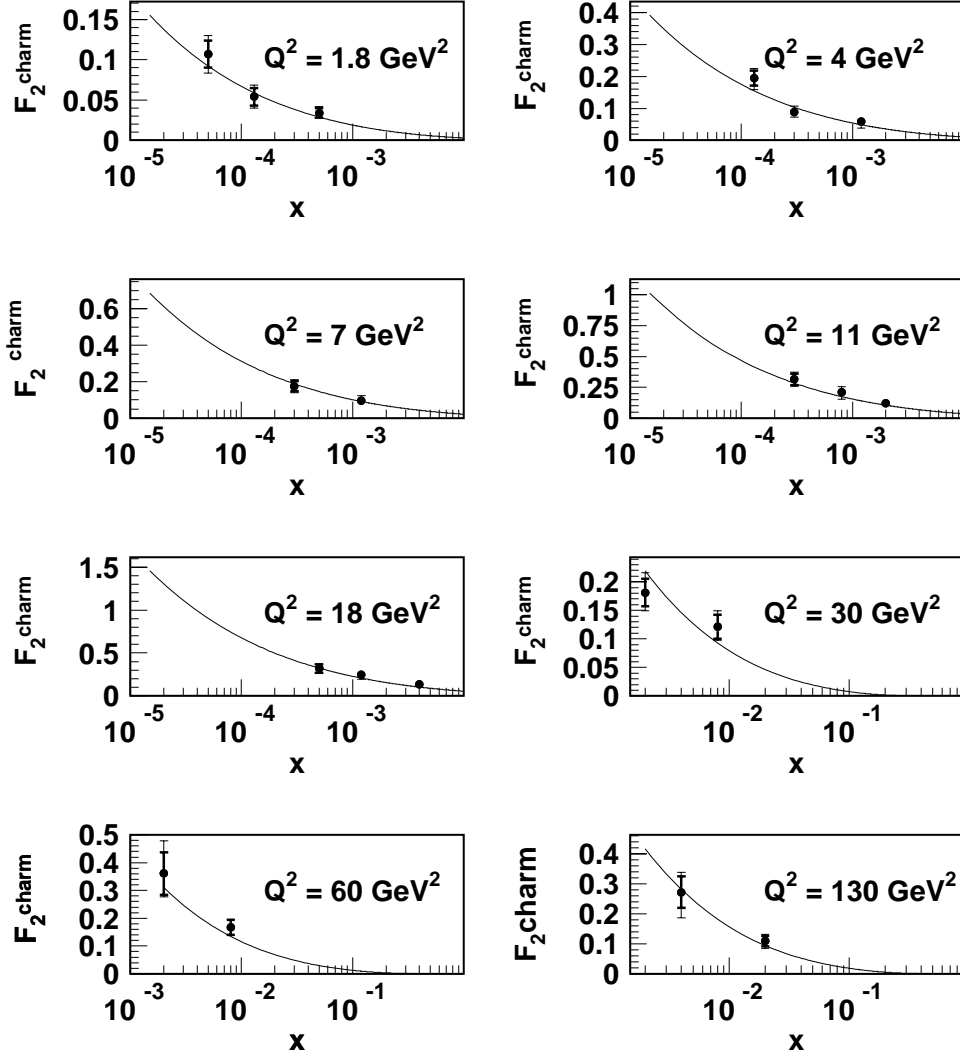


Figure 3.3: The measured F_2^{charm} at Q^2 values between 1.8 and 130 GeV^2 as a function of x . The inner error bars show the statistic errors, the outer error bars the total error. The curves correspond to the calculation of F_2^{charm} by Glück, Reya and Vogt in [8].

$$c_q \equiv c_{p_1} = \frac{Pp_1}{Pq} = -\frac{\hat{u}}{(\hat{s} + Q^2)} \quad (3.42)$$

$$c_g = \frac{Pp_2}{Pq} = -\frac{\hat{t}}{(\hat{s} + Q^2)}, \quad (3.43)$$

where c_q and c_g are related by

$$c_q = 1 - c_g. \quad (3.44)$$

3.3.2 The cross section

In a similar way as done for BGF processes we can calculate the cross section due to QCDC for light quarks (see [5]). In this section we will give a short summary of the

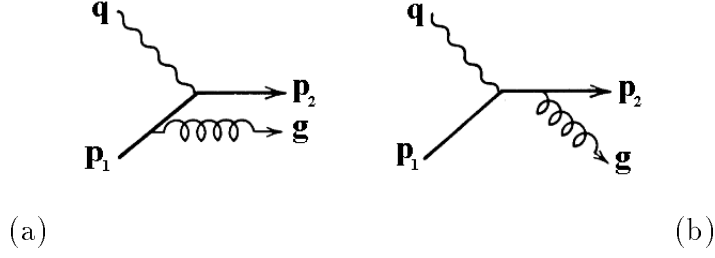


Figure 3.4: *QCD –Compton scattering:*
 (a): *emission of the gluon from the incoming quark,*
 (b): *emission of the gluon from the outgoing quark.*

main results:

For the transverse photons we get the following amplitude:

$$|\mathcal{M}_T|^2 = 64\pi^2\alpha\alpha_s\frac{4}{3}\frac{1}{2}\left[\frac{c_q^2 + z^2}{(1-z)(1-c_q)} + 2(zc_q + 1)\right], \quad (3.45)$$

where $4/3$ is the colour factor and the factor $1/2$ is the average of all possible initial states of quark spins. With eq. (3.19) we get for the contribution of transverse polarized photons to the cross section

$$\hat{\sigma}_T^{QCDC} = \frac{8}{3}\pi\alpha\alpha_s\frac{z}{Q^2}e_q^2\left[\frac{1}{2}\frac{\left(3\beta + 2\log\frac{\beta-1}{-\beta+1}(z^2+1)\right)}{z-1} + \beta(z+1)\right]. \quad (3.46)$$

Using the amplitude for longitudinal photons

$$|\mathcal{M}_L|^2 = 64\pi^2\alpha\alpha_s e_q^2\frac{2}{3}(4zc_q) \quad (3.47)$$

we can calculate the longitudinal contribution. With eq. (3.19) we obtain

$$\hat{\sigma}_L^{QCDC} = \frac{8}{3}\pi\alpha\alpha_s\frac{z}{Q^2}e_q^2[2c_q\beta]. \quad (3.48)$$

We now have to integrate the cross sections in the γq center-of-mass system over the parton densities in order to obtain the contribution from QCD Compton processes to the total cross section. This calculation leads to:

$$\begin{aligned} \sigma^{QCDC} &= \int_{ax}^1 (\hat{\sigma}_L + \hat{\sigma}_T) f_q(\xi, Q^2) d\xi \\ &= \frac{8}{3}\pi\alpha\alpha_s \sum_i \int_{ax}^1 \frac{x}{\xi} \frac{1}{Q^2} C_{\text{light}}^{QCDC} e_q^2 f_q(\xi, Q^2) d\xi, \end{aligned} \quad (3.49)$$

where

$$C_{\text{light}}^{QCDC} = \left[\frac{1}{2}\frac{\left(3\beta + 2\log\frac{\beta-1}{-\beta+1}(z^2+1)\right)}{z-1} + \beta(z+1)\right] + 2c_q\beta, \quad (3.50)$$

where $f_q(\xi, Q^2)$ are the parton densities of up, down and strange quarks and a is defined in eq. (3.32).

Using eq. (3.33) we finally obtain

$$F_2^{\text{light QCDC}} = \frac{Q^2}{4\pi^2\alpha} \sigma^{\text{QCDC}}. \quad (3.51)$$

Due to the dependence on the parton densities, both the integrations of eqs. (3.31) and (3.49) have to be performed numerically. It is problematic that both equations peak for small values of the integrand variable ξ . In order to get a continuous function as result we used the importance sampling transformation method described in appendix A.2.

3.4 The cut off scale p_T

The cross sections for transverse photons for the $\mathcal{O}(\alpha_s)$ corrections introduced by BGF and QCDC processes diverges for $c_q \rightarrow 0$ for BGF and QCDC processes (eqs.(3.25),(3.45), and for $c_{\bar{q}} \rightarrow 0$ for BGF processes (eq.(3.25)). In order to obtain a finite total cross section we are forced to introduce a cut off scale. A possible choice is the transverse momentum p_T in the γ^* parton center-of-mass-system, which we have already used in the previous sections.

A first possibility is to select a minimal p_T such that the sum of $F_2^{\text{light QCDC}}$ and $F_2^{\text{light BGF}}$ is smaller than the total contribution of F_2^{light} .

$$F_2^{\text{light QCDC}} + F_2^{\text{light BGF}} \leq F_2^{\text{light}} \quad (3.52)$$

We computed $F_2^{\text{light BGF}}$ (eq. (3.51)) and $F_2^{\text{light QCDC}}$ (eq. (3.34)) for Q^2 values 100, 150 and 200 GeV² and p_T -cuts between 1 GeV and 1.4 GeV. These structure functions were calculated with leading order parton densities, which originate from fits to the measured total cross section [11], [12]. F_2^{light} calculated with LO parton densities represents the total contribution of the light quarks to the structure function. The p_T -cut values were chosen such that the NLO corrections give the dominant contribution to the structure function F_2^{light} . The result is displayed in fig.(3.4). The following observations are made:

- The smaller the x -values and the higher the Q^2 values are, the higher must the p_T -cut be chosen to avoid that the NLO corrections become bigger than the total structure function F_2^{light} . Only for a p_T -cut of 1.4 GeV the NLO contributions are smaller than the total cross section for all selected Q^2 and x -values.
- The BGF contribution dominates the cross section at small x -values. This is expected due to the high gluon density at low x .

The technique of introducing an artificial p_T -cut such that the sum of $F_2^{\text{light QCDC}}$ and $F_2^{\text{light BGF}}$ is smaller than the total contribution of the light quarks to the structure function is not a satisfactory method of including the $\mathcal{O}(\alpha_s)$ corrections, especially for diffractive DIS: In diffractive DIS the photon interacts with a parton from a gluon dominated object. The quark densities used to calculate the LO contribution are in

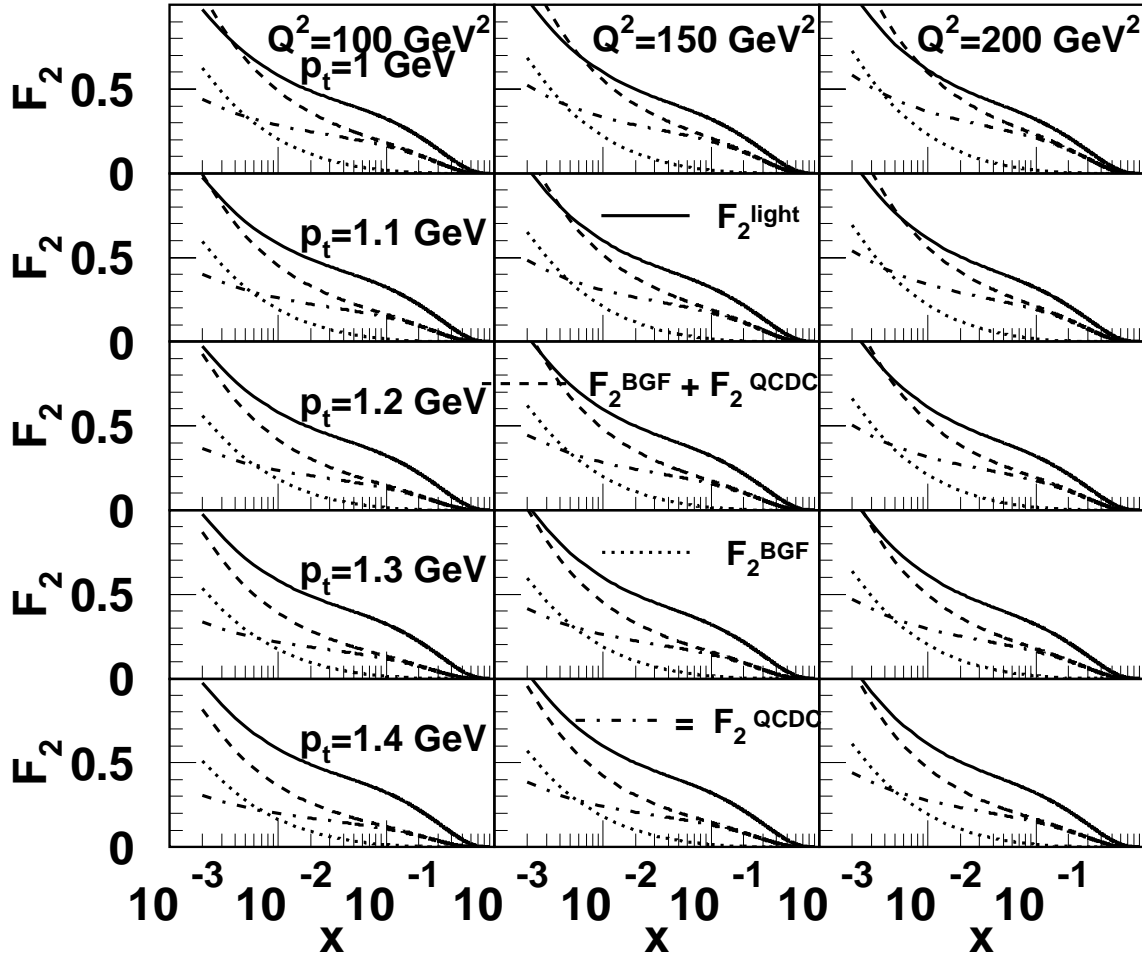


Figure 3.5: Calculated curves for $F_2^{\text{light QCDC}}$, $F_2^{\text{light BGF}}$, the relative sum and F_2^{light} . The distributions are plotted for p_T values from $p_T = 1.1$ to $p_T = 1.4$ GeV.

this case approximately zero, whereas the large gluon density leads to a dominate contribution of BGF processes to the total cross section even at high x -values (see also fig. (5.10) We are therefore forced to introduce large p_T -cuts cutting away large parts of the available phase: jet analysis of the hadronic final state typically start at jet transverse momenta of 3 GeV.

This method of regulating the contributions of NLO corrections by a fixed p_T -cut is inconsistent, as it introduces a critical dependency on the p_T -cut itself: a change in the cut parameter p_T does not imply a change in the corresponding LO parton densities. A consistent way to include the NLO contribution due to BGF into existing Monte-Carlo generator RAPGAP [9] will be described in the next chapter.

Chapter 4

QCD parton shower evolution

In this chapter we will introduce the main aspects of the QCD parton shower evolution used in standard Monte-Carlo generators. We will see that an inclusive summation over all initial states is equivalent to using Q^2 evolved parton structure functions, this Q^2 evolution is based on the Altarelli-Parisi equations.

4.1 The Altarelli–Parisi evolution equation

The partons inside a hadron may be viewed as undergoing a continuous process of branchings and recombinations. At each moment an individual parton c can initiate a cascade, branching into a number of partons. Each generic branching $c \rightarrow ab$ implies some relative transverse momentum between the daughter partons a and b . Energy-momentum conservation requires that at least one of the daughter partons has *space-like virtuality* $m^2 < 0$. Since the partons are virtual, the cascade lives only a finite time before reassembling, with the most off-shell partons living the shortest time. A hard scattering will probe the hadron at a given instant[13]. The probe, i.e the virtual photon, is able to resolve fluctuations in the hadron up to the momentum transfer scale (which for simplicity is taken to Q^2) of the hard scattering [14]. Thus probes at different Q^2 will seem to see different parton compositions in the hadron. The larger the momentum transfer scale in a hard scattering is, the smaller are the distances probed in the hadron and the softer is the observed parton composition. The *change of the parton composition with Q^2 is given by the Altarelli-Parisi (AP) evolution equations*[15]

$$\frac{df_a(x, t)}{dt} = \frac{\alpha_s(t)}{2\pi} \sum_c \int_x^1 \frac{d\xi}{\xi} f_c(\xi, t) P_{c \rightarrow ab}\left(\frac{x}{\xi}\right), \quad (4.1)$$

where

- t is a shorthand for the evolution parameter

$$t = \ln(Q^2) \Rightarrow dt = d\ln(Q^2) = \frac{dQ^2}{Q^2}. \quad (4.2)$$

- $f_i(\xi, t)$ is the parton density for flavour i expressing the probability of finding a parton i carrying a fraction ξ of the total momentum of the hadron, if the hadron

is probed at virtuality Q^2 . The absolute form of the partonic structure functions cannot be predicted by perturbative QCD, but has to be parametrized at some scale Q_0 . Given the parton structure function $f_i(\xi, t)$ at some reference point $t_0 = \ln Q_0^2$, the structure function can then be computed for any Q^2 by the AP-equations.

- $P_{c \rightarrow ab}(z)$ are the AP splitting functions. A parton with momentum fraction x could have come from a quark with larger momentum fraction $\xi > x$. The probability that parton a derives from quark c with $\xi > x$ is proportional to $\alpha_s P_{c \rightarrow ab}$. The splitting function for the process $g \rightarrow q\bar{q}$, which will be of further interest in the following chapters, is given by

$$P_{g \rightarrow q\bar{q}} = \frac{1}{2}(z^2 + (1-z)^2). \quad (4.3)$$

The AP-equations express that, during a small increase dt there is a probability that a parton c with momentum fraction ξ branches into two partons a and b , such that parton a has a fraction $z = x/\xi$ and parton b has a fraction $(1-z)$ of the momentum of parton c .

Correspondingly, during a decrease dt a parton a may be “unresolved” into a parton c . The probability that a parton b disappears from x during a small decrease of the virtuality dt is then given by [16]

$$dP_a = \frac{df_a(x, t)}{f_a(x, t)} \quad (4.4)$$

$$= |dt| \frac{\alpha_s(t)}{2\pi} \sum_a \int_x^1 \frac{d\xi}{\xi} \frac{f_c(\xi, t)}{f_a(x, t)} P_{a \rightarrow bc} \left(\frac{x}{\xi} \right). \quad (4.5)$$

Summing up the cumulative effect of many small changes dt , the probability for no radiation exponentiates. Thus we can define the *Sudakov Form factor*

$$S_a(x, t_{\max}, t) = \exp \left\{ - \int_t^{t_{\max}} dt' \frac{\alpha_s(t')}{2\pi} \sum_a \int_x^1 \frac{d\xi}{\xi} P_{c \rightarrow ab} \left(\frac{x}{\xi} \right) \frac{f_c(\xi, Q'^2)}{f_a(x, Q'^2)} \right\}, \quad (4.6)$$

which gives the probability that a parton a remains at x from t_{\max} to $t < t_{\max}$.

The t value at which the branching $P_{c \rightarrow ab}$ takes place, i.e. the virtuality of a , can be calculated by putting the Sudakov factor $S_a(x, t_{\max}; t)$ equal to a random number between 0 and 1 and solving the equation for t . If the random number is smaller than $S_a(x, t_{\max}; t_0)$ the parton existed at $t_0 = Q_0^2$ and there is no further branching. With eq.(4.2) and $z = x/\xi$ eq. (4.6) can be written as

$$S_a(x, Q_{\max}^2, Q^2) = \exp \left\{ - \int_{Q^2}^{Q_{\max}^2} \frac{dQ'^2}{Q'^2} \frac{\alpha_s(Q'^2)}{2\pi} \sum_c \int_x^1 \frac{dz}{z} P_{c \rightarrow ab}(z) \frac{f_c(x/z, Q'^2)}{f_a(x, Q'^2)} \right\}. \quad (4.7)$$

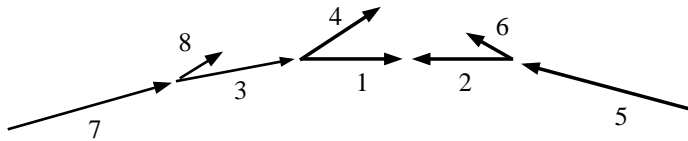


Figure 4.1: Schematic picture of spacelike shower evolution, with hard scattering partons 1 and 2 and emitted timelike partons 4, 6 and 8.

4.2 QCD parton shower evolution

A fast hadron can be viewed as a cloud of quasi real partons [16]. Suppose there is a hard scattering process between two incoming hadrons (or an incoming hadron and an electron, as at HERA), then two partons can be scattered to high p_T such that the partons in the related cascades are provided with the necessary energy to live indefinitely. In principle this energy transfer can be calculated by the corresponding $2 \rightarrow N$ hard scattering matrix elements, where 2 stands for the initiators of the cascades and N for the final parton multiplicity. In practice, it is only possible to calculate the matrix elements for a small number of N .

An alternative approach to include higher order corrections are parton showers (PS's). In the Altarelli-Parisi [15] approximation the partons on the two branches which leads from the two initiators to the hard scattering ($7 \rightarrow 3 \rightarrow 1$) in fig. (4.1) have increasing spacelike virtuality ($Q_7^2 < Q_3^2 < Q_1^2$), adjusted such that all other parton branches (8, 4, 6 in fig. (4.1)) are on mass shell ($M^2 \geq 0$)¹.

The daughter partons (3 and 1) will thus receive transverse momenta greater than that of the initiator 7. The partons on mass shell are called *timelike*, the partons with $M^2 \leq 0$ are called *spacelike*. After the QCD cascade the partons participating in the hard interaction have transverse momenta in contrast to the non parton shower case. The momentum transfer given by the central hard scattering is enough to ensure that all partons may end up on mass shell.

Essentially the partons, except for the two hard scatterers, continue along the direction of the initial parton, but occasionally they can have large transverse momenta giving rise to separately visible jets of their own. In standard Monte Carlo generators is the starting point of the shower evolution the hard scattering subprocess, the evolution is then done backwards from the hard scattering process to the initiators.

Given a parton a one has to find out which branching $c \rightarrow ab$ gave rise to it, alternatively the parton a was already present at the cut-off scale Q_0^2 . This can be done by using AP equations eq. (4.1).

For final state parton showers a forward evolution scheme is used and no parton densities enter the evolution. Details can be found in [17].

¹The virtuality is only one possible ordering criteria of a parton shower, others are e.g. the transversal momentum of the partons, their mass or the angle between the partons.

4.3 Kinematics of the off-shell struck quark

In matrix element calculations all external legs are on mass-shell. The situation is quite the opposite in parton shower algorithms, where the generation of spacelike or timelike masses is a central ingredient. Due to this difference the combined use of matrix element calculations and parton showers is difficult in event generators. In DIS this difference leads to complications in the definition of the variable Björken x [14]: on the one hand Björken x is defined as $x = Q^2/2Pq$ from the kinematics of the lepton vertex, on the other hand Bengtsson and Sjöstrand define in [14] a new variable

$$x_1 = \frac{p_1 q}{Pq}, \quad (4.8)$$

where $p_1(E_1, \vec{p}_1)$ is the four momentum of the struck quark. In the Breit frame, i.e. in the frame where the photon four vector is $q = (0; 0, 0, Q)$, x_1 is the fraction of the longitudinal momentum of the proton (moving in z -direction) carried by the parton. The standard definition of Björken's x and x_1 coincide for massless incoming and outgoing partons, since then

$$\begin{aligned} 0 &= p_1'^2 = (p_1 + q)^2 \\ &= p_1^2 + 2p_1 q + q^2 = x_1 2Pq - Q^2, \end{aligned} \quad (4.9)$$

which implies

$$x_1 = \frac{Q^2}{2Pq} = x. \quad (4.10)$$

If the incoming parton has spacelike virtuality $p_1^2 = Q_1^2$ and/or the outgoing parton a timelike virtuality $p_1'^2 = m_1'^2$, we obtain

$$\begin{aligned} m_1'^2 &= p_1'^2 = (p_1 + q)^2 \\ &= p_1^2 + 2p_1 q + q^2 = x_1 2Pq - Q^2 = -Q_1^2 + x_1 2Pq - Q^2, \end{aligned} \quad (4.11)$$

$$(4.12)$$

which implies

$$x_1 = x \left(1 + \frac{m_1'^2 - Q_1^2}{Q^2} \right) \quad (4.13)$$

in contrast to the standard definition of the parton model $x_1 = x$. Here $m_1'^2 = p_1'^2$ and $Q_1^2 = -p_1^2$ is the virtuality of the exchanged quark. This new definition becomes necessary for the following reason: in the parton model deep inelastic scattering is described by assuming that the incoming and outgoing quarks have small virtualities Q_1^2 and $Q_1'^2 = -p_1'^2$ compared to the virtuality of the photon Q^2 . This approximation is correct for inclusive cross sections, since the hadronic final state is integrated over. Making exclusive calculations this approximation is no longer valid and leads to inconsistent kinematics. The exact choice of energy and momentum combination matters if partons are off mass-shell. On the one hand the usual definition of the structure function $f_a(\xi, Q^2)$ is such that it gives the probability to find a parton with flavour a taking a fraction ξ of the hadron energy or momentum, if the hadron is probed at the scale Q^2 (see section 4.1), so if we deal with structure functions we have to change from

Björken x to the new variable x_1 to treat the kinematics correctly. On the other hand, structure functions are measured experimentally by detecting the scattered lepton, the lepton vertex will then define Björken x . In order to reproduce the correct differential cross section eq. (3.1) one is therefore forced to use the Björken x definition, i.e. that the lepton vertex must be unaffected of the evolution of the parton showers.

In the calculation of the Sudakov form factor eq. (4.7) we assumed that the fractional momentum of the struck quark x_1 equals Björken x , but this assumption is only valid in the limit that masses and virtualities are negligible compared to Q . If m_1^2 and $/$ or $Q_1^2 = -p_1^2$ can not be neglected anymore, one has to use the correct value of the fractional momentum p_1 . The definition of x_1 leads to a change of the Sudakov form factor in eq. (4.7). Bengtsson and Sjöstrand write in [14] a modified Sudakov form factor:

$$S_a^{(\text{BS})}(x, Q_{\text{max}}^2, Q^2) = \exp \left\{ - \int_{Q^2}^{Q_{\text{max}}^2} \frac{dQ'^2}{Q'^2} \frac{\alpha_s(Q'^2)}{2\pi} \sum_c \int_x^1 \frac{dz}{z} P_{c \rightarrow ab}(z) \frac{f_c(x_1/z, Q'^2)}{f_a(x_1, Q'^2)} \right\}. \quad (4.14)$$

4.4 Bengtsson and Sjöstrand algorithm

In the parton shower scheme of Bengtsson and Sjöstrand [14] the four momenta q of incoming photon, p_3 of the incoming gluon, p_1 of the intermediate quark and p'_1 and p_2 of the outgoing quarks obey the following requirements²:

- The proton is to be moving in the $-z$ direction.
- The masses of the outgoing quarks³ as well as the incoming gluon are discarded. Thus:

$$\begin{aligned} (p_1 + q)^2 &= p_1'^2 = 0 \\ (p_3 - p_1)^2 &= p_2^2 = 0 \\ p_3^2 &= 0. \end{aligned}$$

Virtuality Q_1^2 and four momentum p_1 of the intermediate quark are related by

$$p_1^2 = Q^2. \quad (4.15)$$

Bengtsson and Sjöstrand define the scaling variable

$$z_1 = \frac{p_1 \cdot (p_1 + q)}{p_3 \cdot (p_3 + q)}. \quad (4.16)$$

It can be shown (see[2]) that the scattering angle obeys

$$\cos\theta = \frac{p_1^z + q^z}{p_1^0 + q^0} = 1 - \frac{2z_1 Q_1^2 / Q^2}{1 - Q_1^2 / Q^2}. \quad (4.17)$$

²This prescription is implemented in RAPGAP and used by Collins in [2].

³For light quarks the masses of the quarks are small compared to Q^2 and can be neglected.

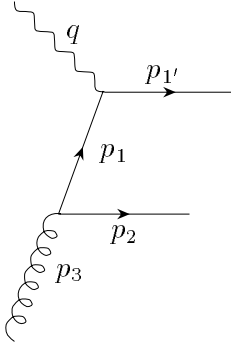


Figure 4.2: A Feynman diagram of the BGF process

The fractional momentum of the gluon is defined to be

$$x_3 = \frac{p_3 \cdot (p_3 + q)}{p \cdot q} = \frac{x}{z_1} \left(1 - \frac{Q_1^2}{Q^2} \right), \quad (4.18)$$

it equals the variable ξ introduced in chapter 3.

The variable z is then (see eq. (3.3))

$$z = \frac{x}{x_3}. \quad (4.19)$$

Neglecting the mass of the outgoing quarks eq. (4.13) can be written as

$$\begin{aligned} x_1 &= x \left(1 - \frac{Q_1^2}{Q^2} \right) \\ &= x - \frac{1}{2} x_3 (1 - \cos\theta), \end{aligned} \quad (4.20)$$

where we have used eq. (4.18). Using the new scheme one has now to deal with a dependence of x_1 on the scattering angle θ .

4.5 Parton shower versus matrix elements

In chapter 3 and this chapter we introduced two possible approaches to include next-to-leading order processes (NLO), i.e. corrections one order higher than the leading order (LO) Born term in an event generator: by higher order matrix elements (ME's) derived by a perturbative expansion of α_s , and/or by parton showers.

The matrix elements of BGF and QCDC in chapter 3, are derived in first order perturbation series of the running coupling constant α_s . Problematic is hereby that the contributions of BGF and QCDC processes to the total cross sections diverge in the collinear region. In order to obtain finite results we are therefore forced to introduce a minimal transvers momentum as cut parameter.⁴

⁴In regularization schemes like the Massive Gluon scheme or the $\overline{\text{MS}}$ scheme finite total cross sections are only obtained by a cancellation between large positive real and large negative virtual contributions.

Furthermore small Q^2 -values lead to big values of the evolution parameter α_s of the QCD perturbation series, making such the perturbation series only slowly divergent in this kinematic region.

Parton showers have complementary strengths: By the resummation of large logarithmic terms in e.g. Sudakov factors, it is possible to obtain a reasonable description also in regions of large α_s values [1]. The disadvantage of the parton shower approach is the crude treatment of wide angle emission, the Feynman diagrams of QCD and BGF may contribute with comparable strengths, and the final cross section may depend on the interference terms between the Feynman diagrams.

Chapter 5

Subtraction method for Boson-Gluon-Fusion

Collins proposes in [2] a method to incorporate BGF processes in a Monte Carlo generator like RAPGAP [9] in a consistent manner. In this chapter we will describe the main aspects of this method¹.

In a Monte Carlo simulator events can either be generated by showering the lowest-order parton model process or the $\mathcal{O}(\alpha_s)$ hard scattering matrix elements (for BGF and QCDC). The first case is suitable to describe the total DIS cross section, neglecting the NLO subprocesses, since they represent only order α_s corrections to the basic process. The second case is e.g. suitable to calculate the production of two-jet events.

Ideally one wants to include in the generation process the LO as well as the NLO contribution. In order to properly describe the phenomenology of diffractive physics it is mandatory to include the gluon induced NLO subprocess. Collins' subtraction method involves the generation of the following two classes of events:

- class 1: events derived in the LO parton model by showering the initial and final state quarks (exactly as at present),
- class 2: events derived by starting with a BGF process and proceeding with the showering².

Between these two classes of events there is no physical distinction, they populate the same regions of phase space, and the events differ only in how the program generates them [2]. The crucial point of Collins' method is that these two classes of events are separated by equipping the cross section for the photon-gluon fusion subprocess with a subtraction that correctly compensates the double counting: the subtraction removes that part of the photon-gluon fusion term that is included in the LO parton model plus showering calculation. The separation is performed by introducing a cut-off function, which depends on the virtuality of the exchanged quarks. This method does the subtractions point by point in the integrand, cancelling out the divergences in the collinear region.

¹The inclusion of QCDC processes is technically more complicated, as in addition to the QCDC compton Feynman graphs the contribution of the virtual corrections have to be taken into account.

²This division of the kinematic regions is very similar to the division obtained in the Massive Gluon scheme, a standard regularization scheme described in appendix B.

In the first section of this chapter we will summarize the basic algorithm used in the event generation at leading order. We will derive the first order contribution to the cross section in the Monte Carlo, from which in section 2 the subtracted gluon-fusion cross section will be computed. This subtracted gluon-fusion can directly implemented in an event generator. The usage of the subtraction method makes mandatory to use appropriate parton densities for this new scheme. In section 3 we will show how this parton densities can be related to $\overline{\text{MS}}$ parton densities and show the LO cross section computed in the scheme appropriate for the subtraction method. Finally we will display the proportion of the LO processes and the contribution of BGF processes in the subtraction method for proton and diffractive parton densities.

5.1 The LO contribution

5.1.1 Basic Monte Carlo algorithm

The basic steps performed by the algorithm used in Monte Carlo generators such as RAPGAP [9] to derive the LO contribution to the cross section are:

1. generate values of x and y (and hence $Q^2 = sxy$) from the LO cross section for DIS eq. (3.1);
2. generate a virtuality Q_1^2 for the incoming quark, a longitudinal momentum fraction z_1 for the first branching, and an azimuthal angle ϕ for this branching. The distributions arise from the Sudakov form factor of eq.(4.14) with $Q^2 = Q_1^2$:

$$S_a^{(\text{BS})}(x, Q_1^2, m_{1'}^2) = \exp \left\{ - \int_{Q_1^2}^{Q_{\text{max}}^2} \frac{dQ'^2}{Q'^2} \frac{\alpha_s(Q'^2)}{2\pi} \sum_c \int_x^1 \frac{dz}{z} P_{c \rightarrow ab}(z) \frac{f_c(x_1/z, Q'^2)}{f_a(x_1, Q'^2)} \right\}. \quad (5.1)$$

The Sudakov form factor is the probability that the virtuality of the struck quark is less than Q_1^2 ;

3. iterate the branching for all initial-state and final-state partons until no further branchings are possible;
4. generate 4-vectors for the momenta of all the generated partons.³

5.1.2 First-order term

The first-order α_s term (the “shower contribution”) is obtained by multiplying the lowest order cross section in eq. (3.1) by the first order term in the expansion of the Sudakov form factor eq. (5.1) in powers of Q^2 . This is made differential in the momenta of the particles involved. As in this work we are interested only in the NLO contribution due to BGF processes, the gluon induced term is selected:

³Only the first two steps of this algorithm will be of further interest in the later sections.

$$\frac{d\sigma^{\text{shower}}}{dx dy dQ_1^2 dz_1 d\phi} = K \sum_a e_a^2 \frac{\alpha_s(Q^2)}{4\pi^2 Q_1^2} C(Q_1^2) P(z_1) \frac{x}{x_1} f_g(x_3, Q^2) \frac{f_a(x)}{f_a(x_1)}, \quad (5.2)$$

where $x_1 = x(1 - Q_1^2)/Q^2$. The splitting kernel P is for $g \rightarrow \text{quark} + \text{antiquark}$

$$P(z_1) = P_{g \rightarrow q\bar{q}}(z_1) = \frac{1}{2}(1 - 2z_1 + 2z_1^2). \quad (5.3)$$

In eq. (5.2) an additional factor $C(Q_1^2)$ has been introduced: this cut-off function $C(Q_1^2)$ gives the maximum value of Q_1^2 for which the shower contribution will be subtracted from the cross section due to BGF processes. It reproduces the upper limit on the Q^2 integral in the Sudakov form factor (eq. (5.1)) and is set to

$$\begin{aligned} C(Q_1^2) &= \theta(Q^2 - Q_1^2) \\ &= 1, \text{ if } Q^2 > Q_1^2 \\ &= 0, \text{ if } Q^2 < Q_1^2 \end{aligned} \quad (5.4)$$

in (5.2).

One might worry that a full Sudakov form factor (without the cut-function) should appear in eq. (5.2) to represent the actual physical suppression of the shower contribution at low Q_1^2 . In fact, the Sudakov form factor should not be used in this formula, since the raison d'être of (5.2) is to be a subtraction term for the NLO contribution to the cross section. The unsubtracted NLO contribution –eq. (5.9) below– has the same singularity and lacks a Sudakov factor. The subtraction will cancel the singularity –see eq. (5.16)– to leave an NLO term that is dominantly in the region of large Q_1^2 [2]. Thus a strict expansion to lowest order in $\alpha_s(Q^2)$ is appropriate, and a resummation of higher-order terms, such as is represented by the Sudakov form factor, is not needed [2].

For later usage we will need the shower contribution in terms of the variables Q_1^2 and $\cos \theta$. From eqs. (4.17) and (4.18) we get

$$Q_1^2 = (1 - \cos\theta)Q^2 \frac{x_3}{2x}, \quad (5.5)$$

$$z_1 = \frac{x}{x_3} - \frac{1}{2}(1 - \cos\theta). \quad (5.6)$$

Then the Jacobian of the transformation is given by

$$\frac{\partial(x_3, \cos\theta)}{\partial(z_1, Q_1^2)} = \frac{2x}{z_1 Q^2}. \quad (5.7)$$

From eq. (5.2) we get then

$$\begin{aligned} \frac{d\sigma_{\text{shower}}^{(\text{BS})}}{dx dy dx_3 d\cos\theta d\phi} &= K \sum_a e_a^2 \frac{\alpha_s(Q^2)}{4\pi^2} C(Q_1^2) \frac{x}{x_3} f_g(x_3, Q^2) \frac{f_a(x)}{f_a(x_1)} \times \\ &\quad \times \frac{1}{1 - \cos\theta} P\left(\frac{x}{x_3} - \frac{1}{2}(1 - \cos\theta)\right). \end{aligned} \quad (5.8)$$

5.2 Boson-gluon fusion with subtraction

From the matrix elements of BGF for transversal and longitudinal photons in eqs. (3.9) and (3.27) we can derive a fivefold differential cross section due to BGF ([7], [2]). Later on, this differential cross section will be called “unsubtracted”, as we will subtract from this cross section the contribution due to the shower algorithms eq. (5.8).

$$\frac{d\sigma_{\text{unsubtracted}}(F_2 \text{ part})}{dx dy dx_3 d\cos\theta d\phi} = K \sum_{\text{quarks } a} e_a^2 \frac{\alpha_s(Q^2)}{4\pi^2} \frac{x}{x_3} f_g(x_3, Q^2) \left\{ P(z) \left[\frac{1}{1 - \cos\theta} + \frac{1}{1 + \cos\theta} \right] - \frac{1}{2} + 3z(1 - z) \right\}. \quad (5.9)$$

This unsubtracted photon-gluon fusion differential cross section diverges as $|\cos\theta| \rightarrow 1$, thus the integration can not be performed over the full kinematic range. This divergences are illustrated in fig. (5.1), where the differential cross section due to BGF eq.(5.9) is plotted with simplified quark and gluon densities $f_a(x) = (1 - x)^5/x$ against $\cos\theta$ at fixed x , x_3 and Q^2 values.

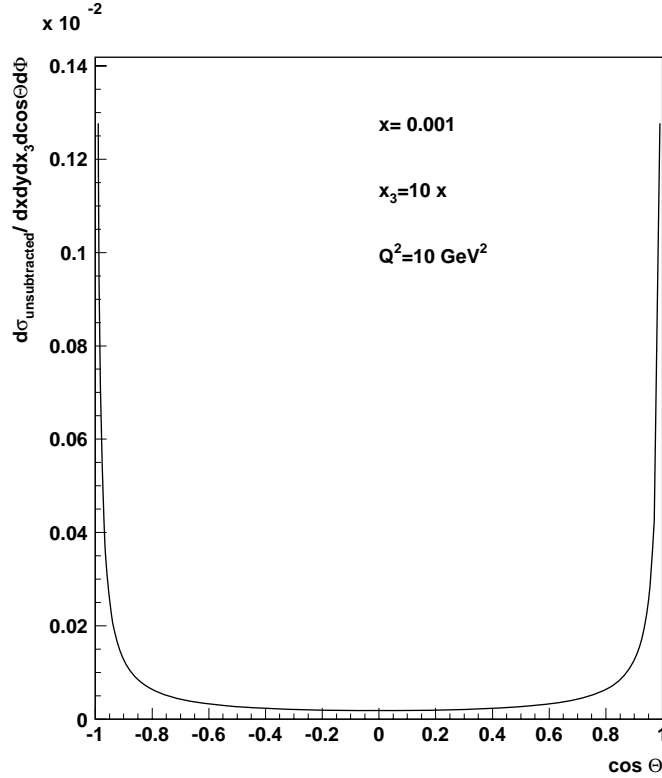


Figure 5.1: The differential cross section due to BGF eq. (5.9) plotted with simplified parton densities for fixed values of $x = 0.001$, $x_3 = 10x$, $Q^2 = 10 \text{ GeV}^2$.

To avoid double counting between events generated by starting with the BGF matrix elements eq. (5.9) and events derived by showering the LO contribution (the

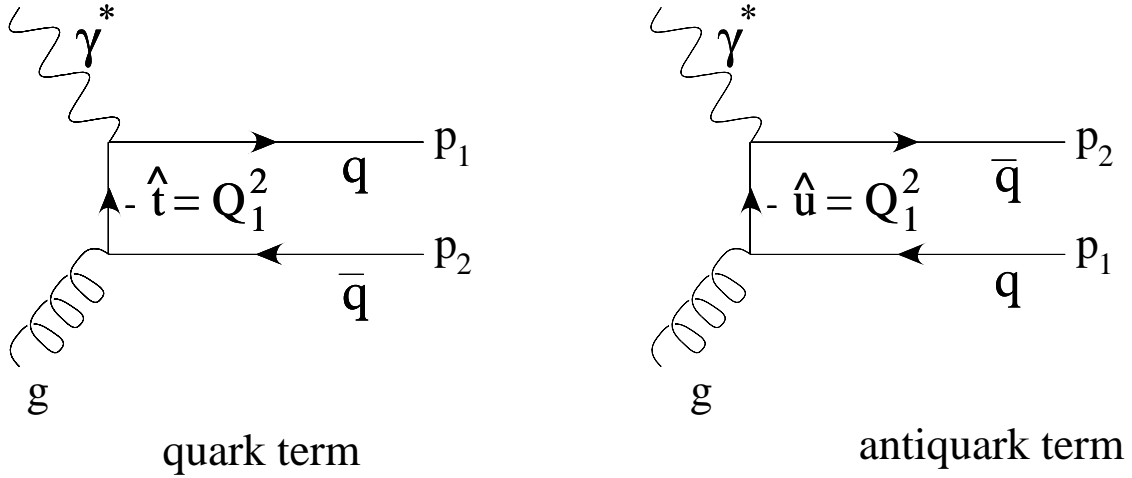


Figure 5.2: Feynman graphs of BGF processes: the momentum exchange between incoming gluon and photon is for the quark term in the t -channel, for the antiquark in the u -channel.

“shower terms”) eq. (5.8) we must now subtract the shower contribution from the boson gluon contribution. The shower contribution eq. (5.8) can be divided into contributions from quarks and antiquarks by treating the antiquark as a quark term with θ replaced by $\pi - \theta$.

For the quark term the momentum exchange between the incoming virtual photon and the scattered quark is in the t -channel (see eq. (5.5) and fig. (5.2)), thus we get from eq. (5.5)

$$p_1^2 = t = -Q_1^2 = -Q^2(1 - \cos\theta)x_3/2 \quad (5.10)$$

leading to

$$\begin{aligned} \frac{d\sigma_{\text{shower, quarks}}^{(\text{BS})}}{dx dy dx_3 d\cos\theta d\phi} &= K \sum_{\text{quarks } a} e_a^2 \frac{\alpha_s(Q^2)}{4\pi^2} C(-t) \frac{x}{x_3} f_g(x_3, Q^2) \frac{f_a(x)}{f_a(x_{1t})} \times \\ &\times \frac{1}{1 - \cos\theta} P\left(\frac{x}{x_3} - \frac{1}{2}(1 - \cos\theta)\right), \end{aligned} \quad (5.11)$$

where x_{1t} is the value of the scaling variable x_1 (eq. 4.20) for the quark term,

$$x_{1t} = x \left(1 + \frac{t}{Q^2}\right). \quad (5.12)$$

The subscript “quarks a” indicates that we sum only over the quark flavours. For the antiquark term is the momentum exchange between the incoming virtual photon and the scattered quark in the u -channel (see fig.(5.2)), thus

$$p_1^2 = u = -Q_1^2 = -Q^2(1 + \cos\theta)x_3/2x \quad (5.13)$$

From eq. (4.20) follows then for the scaling variable x_1 in the case of antiquarks

$$x_{1u} = x \left(1 + \frac{u}{Q^2}\right) \quad (5.14)$$

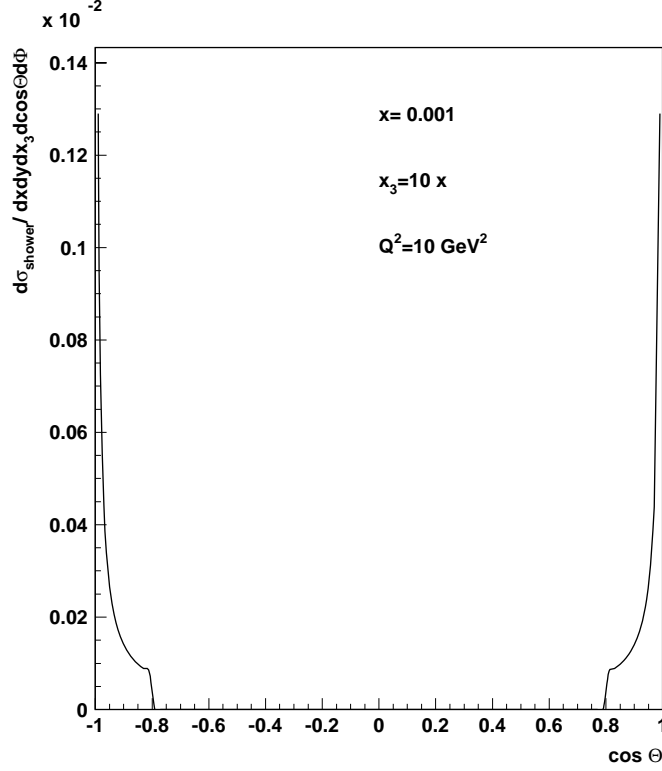


Figure 5.3: The differential cross section due to the shower algorithm (5.8) plotted with simplified parton densities for fixed values of $x = 0.001$, $x_3 = 10x$ and $Q^2 = 10 \text{ GeV}^2$.

leading to

$$\begin{aligned} \frac{d\sigma_{\text{shower, antiquarks}}^{(\text{BS})}}{dx dy dx_3 d\cos \theta d\phi} &= K \sum_{\text{quarks } a} e_a^2 \frac{\alpha_s(Q^2)}{4\pi^2} C(-u) \frac{x}{x_3} f_g(x_3, Q^2) \frac{f_{\bar{a}}(x)}{f_{\bar{a}}(x_{1u})} \times \\ &\times \frac{1}{1 + \cos \theta} P \left(\frac{x}{x_3} - \frac{1}{2}(1 + \cos \theta) \right), \end{aligned} \quad (5.15)$$

where we have used $e_a^2 = e_{\bar{a}}^2$. We have to take into account that in eqs. (5.11) and (5.15) the sum is only over the quarks, not the antiquarks flavours.

The shower contribution shows the same divergences as the BGF matrix element for $|\cos \theta| \rightarrow 1$. This is shown in fig. (5.3) where we plotted the sum of eq. (5.11) and eq. (5.15) against $\cos \theta$ with the same parameters as in fig. (5.1).

The shower terms eqs. (5.11) and (5.15) must be subtracted from eq. (5.9) in order to avoid double counting between the two classes of events – on one hand events generated by the shower terms, on the other hand events deriving from the BGF matrix elements:

$$\begin{aligned}
\frac{d\sigma_{\text{hard}}^{(\text{BS})}(F_2 \text{ part})}{dx dy dx_3 d\cos\theta d\phi} &= K \sum_{\text{quarks } a} e_a^2 \frac{\alpha_s(Q^2)}{4\pi^2} \frac{x}{x_3} f_g(x_3, Q^2) \\
&\left\{ \frac{1}{1 - \cos\theta} \left[P(z) - C(-t) \frac{f_a(x)}{f_a(x_{1t})} P\left(z - \frac{1}{2}(1 - \cos\theta)\right) \right] \right. \\
&\quad + \frac{1}{1 + \cos\theta} \left[P(z) - C(-u) \frac{f_{\bar{a}}(x)}{f_{\bar{a}}(x_{1u})} P\left(z - \frac{1}{2}(1 + \cos\theta)\right) \right] \\
&\quad \left. - \frac{1}{2} + 3z(1 - z) \right\}. \tag{5.16}
\end{aligned}$$

By subtracting the shower contribution from the unsubtracted differential cross sections the divergence for $|\cos\theta| \rightarrow 1$ has been cancelled out. This is explained more detailed for the quark term: if $\cos\theta \rightarrow 1$ then $x = x_{1t}$, and for $-t > Q^2$ (that is the kinematic range for which we want to calculate the NLO correction) the square bracket becomes 0. Similar argumentation holds for $\cos\theta \rightarrow -1$ for the antiquark term. In fig. (5.4) we show that by subtraction of the shower term from the boson gluon cross section the divergences cancel.

The purpose of introducing a cut-off function is to obtain the correct cross section when $Q_1^2 \ll Q^2$, that is the region where the cross section is dominated by the shower algorithm. The cut-off function creates two kinematic regions (see fig. (5.5)):

- $Q^2 > Q_1^2$: the dominant contribution to the cross section (and F_2) derives from the shower algorithm. The shower contribution eq.(5.8) will be subtracted from the BGF NLO contribution reflecting the physical suppression of NLO contributions in this kinematic region;
- $Q^2 < Q_1^2$: in this kinematic region NLO corrections give the dominant contribution, the shower contribution is 0.

There is some freedom in choosing the cut-off function, as any change in the cut-off function is compensated by the corresponding changes in the subtraction terms, up to errors of yet higher order in $\alpha_s(Q^2)$. In order to do useful calculations the cut-off function should be chosen such that higher-order corrections, like eq. (5.16), are not excessively large. In this work the standard case $C(Q_1^2) = \theta(Q^2 - Q_1^2)$ was implemented in the programs which calculate the F_2^{BGF} . For the implementation in a Monte Carlo generator like RAPGAP [18] this choice is very convenient, as the standard Sudakov Factor (eq. (4.14)) can be used.

5.2.1 Computing of $F_2^{\text{BGF, hard}}$

With Collins' subtraction method the contribution of the $\mathcal{O}(\alpha_s)$ correction of BGF processes to the structure function F_2^{BGF} is divided in a part generated by the shower algorithm F_2^{shower} and the hard contribution obtained by subtracting the shower contribution from the full matrix element contribution F_2^{hard}

$$F_2^{\text{BGF}} = F_2^{\text{shower}} + F_2^{\text{hard}}. \tag{5.17}$$

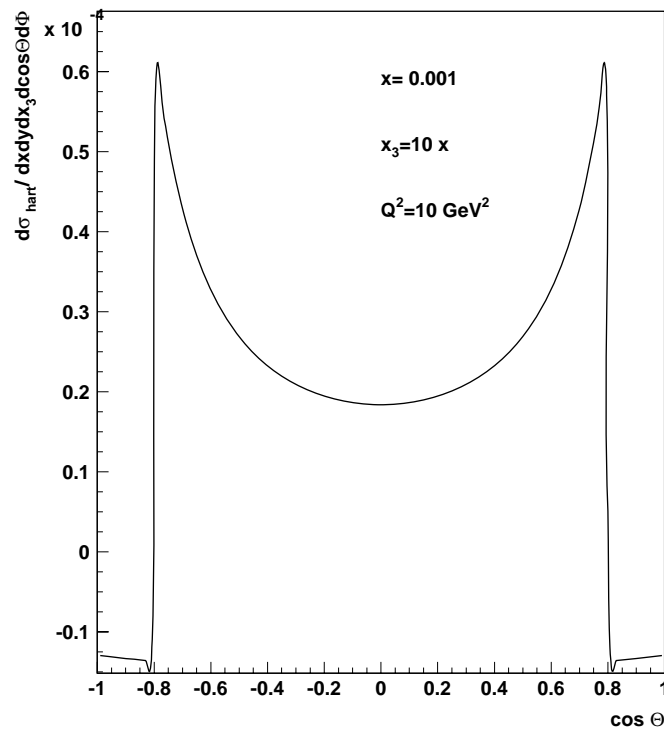


Figure 5.4: The differential hard cross section eq. (5.16) plotted with simplified parton densities $f_a = (1-x)^5/x$ for fixed values of $x = 0.001$, $x_3 = 10x$ and $Q^2 = 10 \text{ GeV}^2$.

The division between both contributions is made by the dynamic cut parameter Q_1^2 , which sets the shower contribution F_2^{shower} to 0, if $Q_1^2 > Q^2$. The cut parameter Q_1^2 depends on the kinematics of each single event. This is an important difference to the fixed cut parameter p_T introduced in chapter 3. Fig. (5.5) illustrates the role of Q_1^2 as cut parameter.

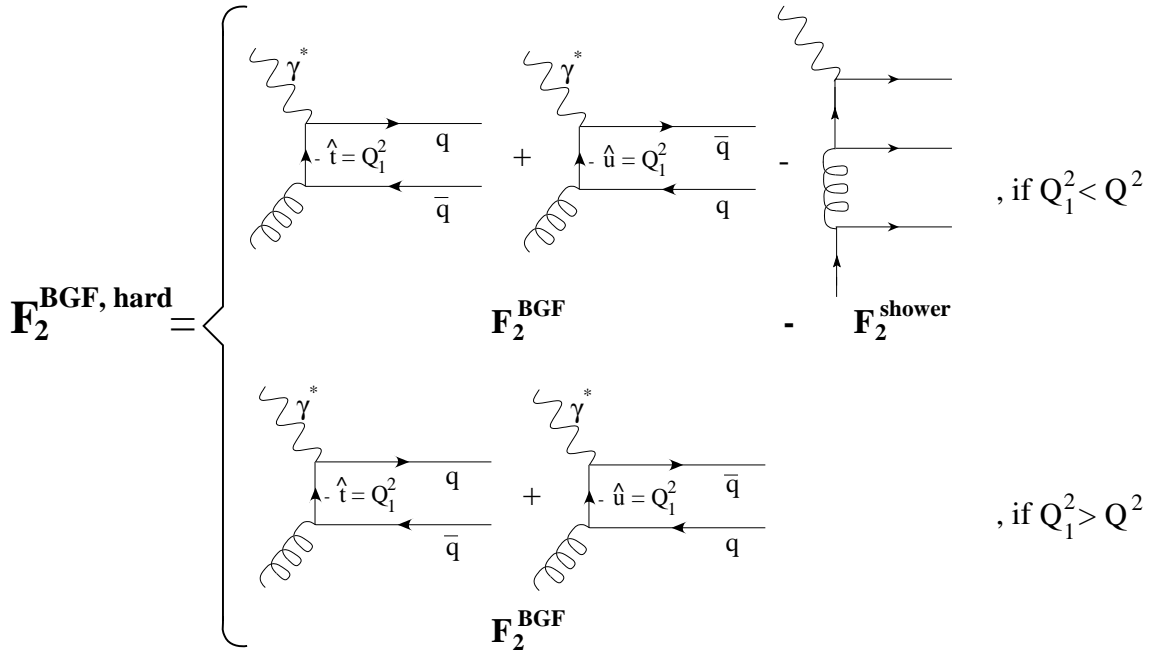


Figure 5.5: Terms contributing to $F_2^{\text{BGF, hard}}$: if $Q_1^2 < Q^2$ $F_2^{\text{BGF, hard}}$ is generated by subtracting the shower terms from the matrix elements, if $Q_1^2 > Q^2$ then $F_2^{\text{BGF, hard}}$ is generated only by the matrix element contribution.

By integrating eqs.(5.9), (5.8) and (5.16) over x_3 , $\cos \theta$ and ϕ we can now compute F_2^{BGF} , F_2^{shower} and F_2^{hard} . The connection between $d\sigma/dxdy$ and F_2 is given by eq. (2.12). Whereas the integration over ϕ leads to a factor 2π , both the integrations over x_3 and $\cos \theta$ have to be performed numerically: the integration over x_3 due to the dependence on the gluon density $f_g(x_3)$, the $\cos \theta$ integrations due to the dependence on $x_1 = x - \frac{1}{2}x_3(1 - \cos \theta)$ of the structure function $f_a(x_1)$ (see section 4.4).⁴ It should be stressed that *in the hard contribution* eq. (5.16) the divergence in $\cos \theta$ is cancelled out, therefore *no cut in $\cos \theta$ has to be made* in order to calculate the hard contribution of BGF, it can be calculated over the whole phase space. The integration over ξ is numerically demanding, as the integrands in eqs. (5.9), (5.8) and (5.16) are proportional to $1/\xi$, thus the integrand peaks for small ξ values. This behaviour of the integrands makes a numeric integration very difficult. In order to

⁴From eqs. (5.9), (5.11) and (5.15) we see that the differential cross section of the unsubtracted BGF as well as the shower terms diverge for $|\cos \theta| \rightarrow 1$. We were therefore forced to introduce a cut in $\cos \theta$ for the calculation of the cross section of the shower terms resp. the unsubtracted BGF, we accepted only $\cos \theta$ values with $|\cos \theta| < 0.999999$. This minimal cut in $\cos \theta$ cuts only a few events and it has no significant effects on the obtained results. This cut in $\cos \theta$ has no effect on the later implementation in the Monte Carlo, as only the hard contribution will be included in the generation.

get a continuous result for the physical cross section we used for the ξ -integration the *importance sampling method* described in appendix A.2. This transformation method was also used for the $\cos \theta$ integration of the unsubtracted contribution and the shower terms⁵. We integrated eqs. (5.9), (5.8) and (5.16) over ϕ (leading to a general factor 2π), x_3 and $\cos \theta$ and calculated the cross section as function of Bjørken x and Q^2 . The Bjørken x -values were chosen between 10^{-4} and 10^{-1} , while the Q^2 -values were chosen between 5 and 100 GeV². The result of the integration of the unsubtracted BGF cross section, the shower term, and the hard contribution (the difference of both terms) is plotted in figure (5.6).

It can be seen that for all Q^2 values the hard cross section is only a small percentage (about 10 %) of the total contribution of BGF to the structure function, the rest of the contribution of BGF to the total cross section is derived by showering the LO Born term (see the following section 5.3). That means that in most cases the shower contribution is subtracted from the unsubtracted cross section in order to compute $F_2^{\text{BGF, hard}}$, as for most cases Q_1^2 is smaller than Q^2 . From fig. (5.6) we see that the cross sections can not be calculated for all Q^2 over the whole x -range: the higher the Q^2 values are the smaller the higher is the first x value for which the cross section can be calculated. This can be explained by the fact that the scaling variable

$$y = Q^2/xs, \quad (5.18)$$

where s is the square of the available center of mass energy, must be smaller than 1 for each event (see eq. (2.4)). We have chosen $\sqrt{s} = 320$ GeV, this is the center of mass energy available at HERA.

5.2.2 Diffractive DIS

In diffractive DIS processes the photon interacts with a parton which carries a fraction β of the momentum of the pomeron⁶. The subtraction method can easily be applied to diffractive DIS. To do this the parton densities in the above formula have to be replaced by diffractive parton densities and Bjørken x has to be replaced by β . We used the diffractive parton densities parametrized in [20]. This diffractive parton densities are only available in the following kinematic range:

$$\beta = 0.01\dots 1, \quad Q^2 = 3\dots 100 \text{ GeV}^2. \quad (5.19)$$

From figure (5.7) we can see that also in the diffractive case the hard contribution is only a small part (about 10 %) of the the full contribution of BGF to the structure function. This is not astonishing, as in both cases the same cut-function $C(Q_1^2)$ was used in order to separate the shower contribution from the matrix element contribution.

⁵Details of the x_3 -transformation can be found in appendix A.2.1, of the $\cos \theta$ -integration in appendix A.2.2.

⁶The pomeron is a colour neutral object which is emitted by the proton. A detailed description of the kinematics of diffractive processes can be found in [19].

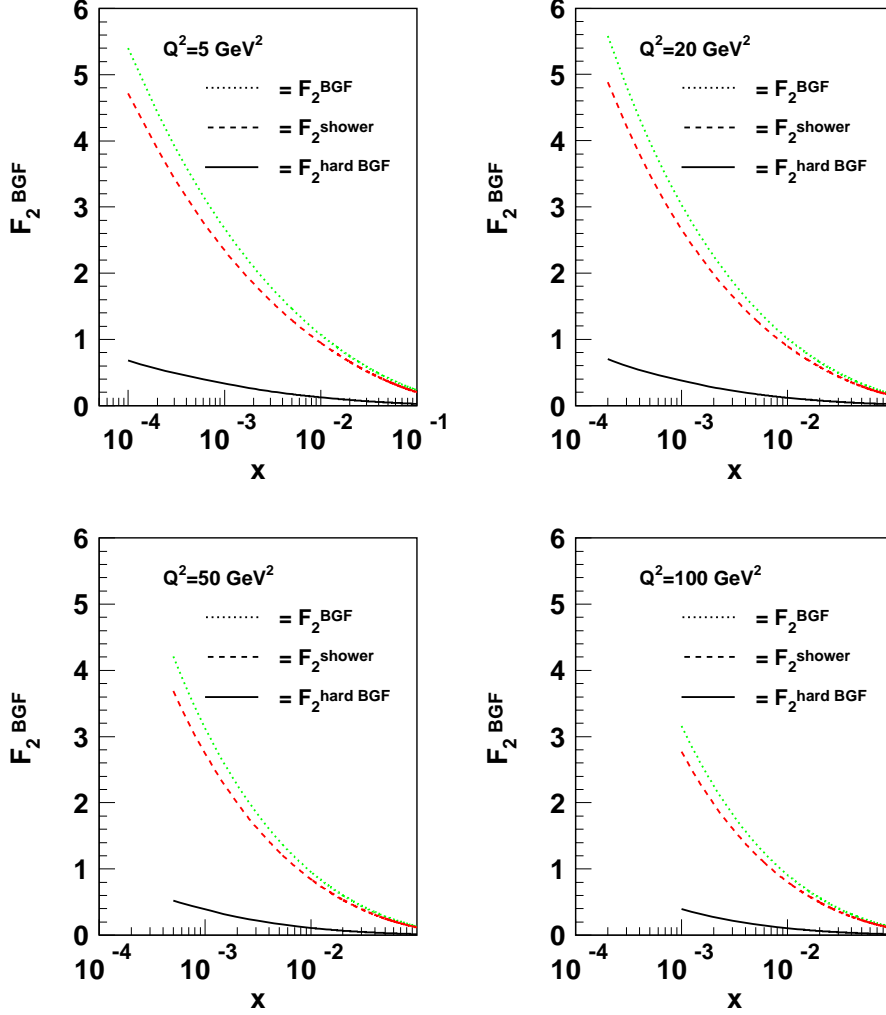


Figure 5.6: F_2^{BGF} calculated by the full matrix element, F_2^{shower} due to the shower algorithm and $F_2^{\text{BGF, hard}}$ calculated by Collins' subtraction method. The $\overline{\text{MS}}$ parton densities have been used to calculate the structure functions.

5.3 Comparison with $\overline{\text{MS}}$ scheme

In order to implement the above algorithm in an event generator, it is mandatory to find out which parton densities are required to calculate eq. (5.16). The usage of the correct parton densities is an important question, as the numerical value of the parton densities can be changed at order α_s and beyond by a change of scheme. The aim is to find a process-independent relation between parton densities in the scheme appropriate for the subtraction method the Bengtson and Sjöstrand (BS) scheme and a standard regularization scheme. Standard fits to parton densities are typically made in the $\overline{\text{MS}}$ (Minimal Subtraction) scheme. Therefore it is necessary to find a relation between the

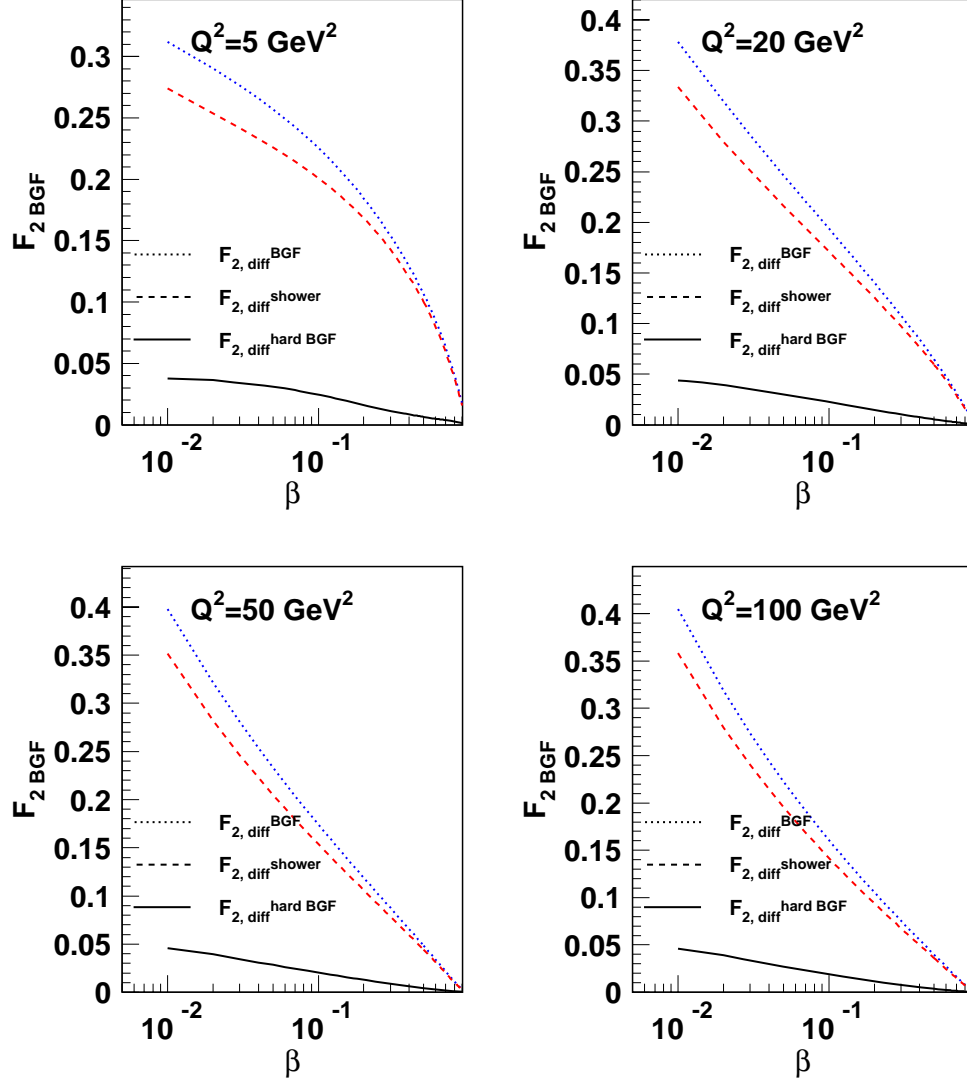


Figure 5.7: F_2^{BGF} , $F_2^{\text{BGF hard}}$ and F_2^{shower} in diffraction. The structure functions are calculated with diffractive parton densities and plotted against the diffractive scaling variable β .

$\overline{\text{MS}}$ scheme to the scheme used in the event generator.

This relation can be found by integrating the BS-scheme cross section over the hadronic final state and requiring that the obtained result is the same as in the standard factorization approach with $\overline{\text{MS}}$ parton densities. From the above calculation for the structure we obtain

$$F_2^a(x, Q^2) = \sum_a x e_a^2 f_a^{(\text{BS})}(x, Q^2)$$

$$\begin{aligned}
& + \frac{\alpha_s(Q^2)}{2\pi} \sum_{\text{quarks } a} \int_x^1 dx_3 \int_{-1}^1 d\cos\theta \frac{x}{x_3} f_g^{(\text{BS})}(x_3, Q^2) \times \\
& \left\{ \frac{1}{1 - \cos\theta} \left[P(z) - C(-t) \frac{f_a^{(\text{BS})}(x)}{f_a^{(\text{BS})}(x_1)} P\left(z - \frac{1}{2}(1 - \cos\theta)\right) \right] \right. \\
& \quad \left. - \frac{1}{4} + \frac{3}{2}z(1 - z) \right\} \\
& + \mathcal{O}(\alpha_s) \text{ quark terms} + \mathcal{O}(\alpha_s^2) \\
= & F_2^{\text{LO}} + F_2^{\text{BGF, hard}} + \mathcal{O}(\alpha_s^2). \tag{5.20}
\end{aligned}$$

The first term in eq. (5.20) is the LO contribution (see eq. (2.12)), the summation has to be performed over quark and antiquark flavours. The superscripts on the quark densities indicate that they are in the scheme appropriate for the Bengtsson-Sjöstrand algorithm. The second term is $F_2^{\text{BGF, hard}}$, the ‘‘hard contribution’’, derived by the subtraction method. In the ‘‘ $\mathcal{O}(\alpha_s)$ quark terms’’ are the remaining $\mathcal{O}(\alpha_s)$ corrections, QCDC and the virtual corrections, included. We are looking for a process-independent relation between parton densities, and we want a result for each quark flavour and not just the combination that appears in the usual electromagnetic F_2 . It is convenient to replace the actual structure function eq.(5.20) by one in which the photon couples only to one flavor of quark, with unit coupling. This leads to

$$\begin{aligned}
F_2^a(x, Q^2) & = x f_a^{(\text{BS})}(x, Q^2) \\
& + \frac{\alpha_s(Q^2)}{2\pi} \int_x^1 dx_3 \int_{-1}^1 d\cos\theta \frac{x}{x_3} f_g^{(\text{BS})}(x_3, Q^2) \times \\
& \left\{ \frac{1}{1 - \cos\theta} \left[P(z) - C(-t) \frac{f_a^{(\text{BS})}(x)}{f_a^{(\text{BS})}(x_1)} P\left(z - \frac{1}{2}(1 - \cos\theta)\right) \right] \right. \\
& \quad \left. - \frac{1}{4} + \frac{3}{2}z(1 - z) \right\} \\
& + \mathcal{O}(\alpha_s) \text{ quark terms} + \mathcal{O}(\alpha_s^2). \tag{5.21}
\end{aligned}$$

Comparing eqs. (5.21) and (5.20) we see that in eq. (5.21) the last two terms in the curly brackets are only one half of the last two terms in eq.(5.20). In eq. (5.20) the contribution of quarks and antiquarks for each flavour was calculated, while in eq. (5.21) we want to calculate a hypothetical F_2^a with unit coupling to one flavour of quark, not regarding the corresponding antiquark contribution.

Next we take the formula for the structure function with $\overline{\text{MS}}$ parton densities [3]. Again we display the actual cross section by the one in which the photon couples to only one flavour of quark with unit coupling

$$\begin{aligned}
F_2^a(x, Q^2) & = x f_a^{(\overline{\text{MS}})}(x, \mu^2) \\
& + \frac{\alpha_s(\mu^2)}{2\pi} \int_x^1 dx_3 \frac{x}{x_3} f_g^{(\overline{\text{MS}})}(x_3, \mu^2) \left[P(z) \log \frac{Q^2(1 - z)}{\mu^2 z} - \frac{1}{2} + 4z(1 - z) \right] \\
& + \mathcal{O}(\alpha_s) \text{ quark terms} + \mathcal{O}(\alpha_s^2). \tag{5.22}
\end{aligned}$$

Eq. (5.22) equals eq. (5.20), as the physical cross section must be scheme independent.

In order to calculate the connection between the parton densities in both schemes we must take into account the following relations for the parton densities in the BS scheme and the $\overline{\text{MS}}$ scheme:

$$f_g^{\text{BS}}(x, Q^2) = f_g^{\overline{\text{MS}}}(x, Q^2) + \mathcal{O}(\alpha_s) \quad (5.23)$$

$$f_q^{\text{BS}}(x, Q^2) = f_q^{\overline{\text{MS}}}(x, Q^2) + \mathcal{O}(\alpha_s), \quad (5.24)$$

where we have set $Q^2 = \mu^2$. In eqs. (5.22) and (5.20) there is a factor α_s in the $\mathcal{O}(\alpha_s)$ contributions, thus the error we make by the approximation $f_g^{\text{BS}}(x, Q^2) = f_g^{\overline{\text{MS}}}(x, Q^2)$ and $f_q^{\text{BS}}(x, Q^2) = f_q^{\overline{\text{MS}}}(x, Q^2)$ is of order α_s^2 . Therefore it is justified to use in both schemes the $\overline{\text{MS}}$ parton densities for the terms originating from order α_s corrections. This approximation can not be made for the contribution from the lowest order Feynman graph $\gamma^* q \rightarrow q$ in eq. (5.20), as this term is of zeroth order α_s . In order to calculate F_2 we are therefore forced to find the connection between the parton densities in the $\overline{\text{MS}}$ scheme and the BS scheme. As the cross section is scheme independent, we obtain

$$\begin{aligned} x f_a^{(\text{BS})}(x, Q^2) &= x f_a^{(\overline{\text{MS}})}(x, \mu^2) \\ &+ \frac{\alpha_s(\mu^2)}{2\pi} \int_x^1 dx_3 \frac{x}{x_3} f_g^{(\overline{\text{MS}})}(x_3, \mu^2) \\ &\times \left\{ P(z) \log \frac{Q^2(1-z)}{\mu^2 z} + z(1-z) \right. \\ &\quad \left. - \int_{-1}^1 \frac{d\cos\theta}{1-\cos\theta} \left[P(z) - C(-t) \frac{f_a(x)}{f_a(x_1)} P\left(z - \frac{1}{2}(1-\cos\theta)\right) \right] \right\} \\ &+ \mathcal{O}(\alpha_s) \text{ quark terms} + \mathcal{O}(\alpha_s^2). \end{aligned} \quad (5.25)$$

The connection between the parton densities in the $\overline{\text{MS}}$ scheme and the BS scheme is a quite unpleasant formula and two additional numeric integrations have to be performed to find the relation between these schemes. In fig. (5.8) we show the leading order contribution

$$F_2^{\text{LO}} = \sum_a x e_a^2 f_a(x, Q^2) \quad (5.26)$$

calculated with parton densities in the $\overline{\text{MS}}$ and the BS scheme for Q^2 values between 5 and 100 GeV² ⁷.

Whereas for x -values greater than 0.11 there is no significant difference between the LO contributions F_2^{LO} in the $\overline{\text{MS}}$ and BS scheme, there is a clear difference between both schemes for smaller x -values. F_2^{LO} calculated in the BS-scheme is up to 20% bigger than the corresponding F_2^{LO} in the $\overline{\text{MS}}$ scheme.

Fig. (5.8) demonstrates thus that the implementation of the subtraction method in an event generator makes mandatory to use the parton densities appropriate for the BS scheme.

⁷For the ξ -integration we used again the transformation method describe in section A.2.1.

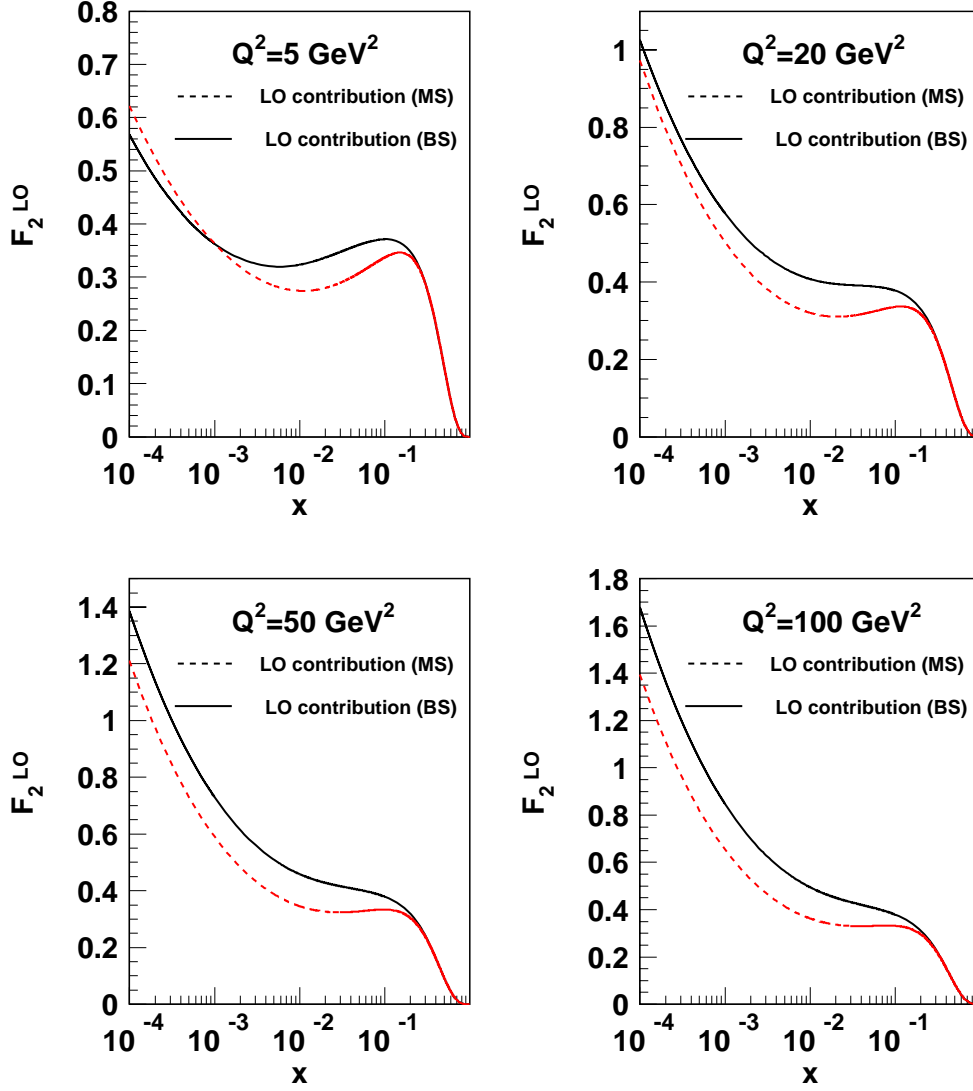


Figure 5.8: Leading order contribution to F_2 calculated with parton densities in the $\overline{\text{MS}}$ scheme and the BS scheme.

In eq. (5.20) we calculated F_2 in the new BS scheme. The LO contribution as well as the hard contribution F_2^{BGF} to F_2 are plotted in figure (5.9)⁸. The higher the x -values are, the lower are the gluon densities. This explains that F_2^{BGF} becomes bigger with increasing x -values.

Furthermore we see that the percentage of the LO contribution F_2^{BGF} to the sum of LO and hard contribution becomes smaller with decreasing Q^2 . For the lowest plotted Q^2 value of 5 GeV^2 $F_2^{\text{BGF hard}}$ becomes even smaller than the hard contribution

⁸ F_2^{LO} is calculated with the parton densities in the BS scheme, F_2^{BGF} with parton densities in the $\overline{\text{MS}}$ scheme.

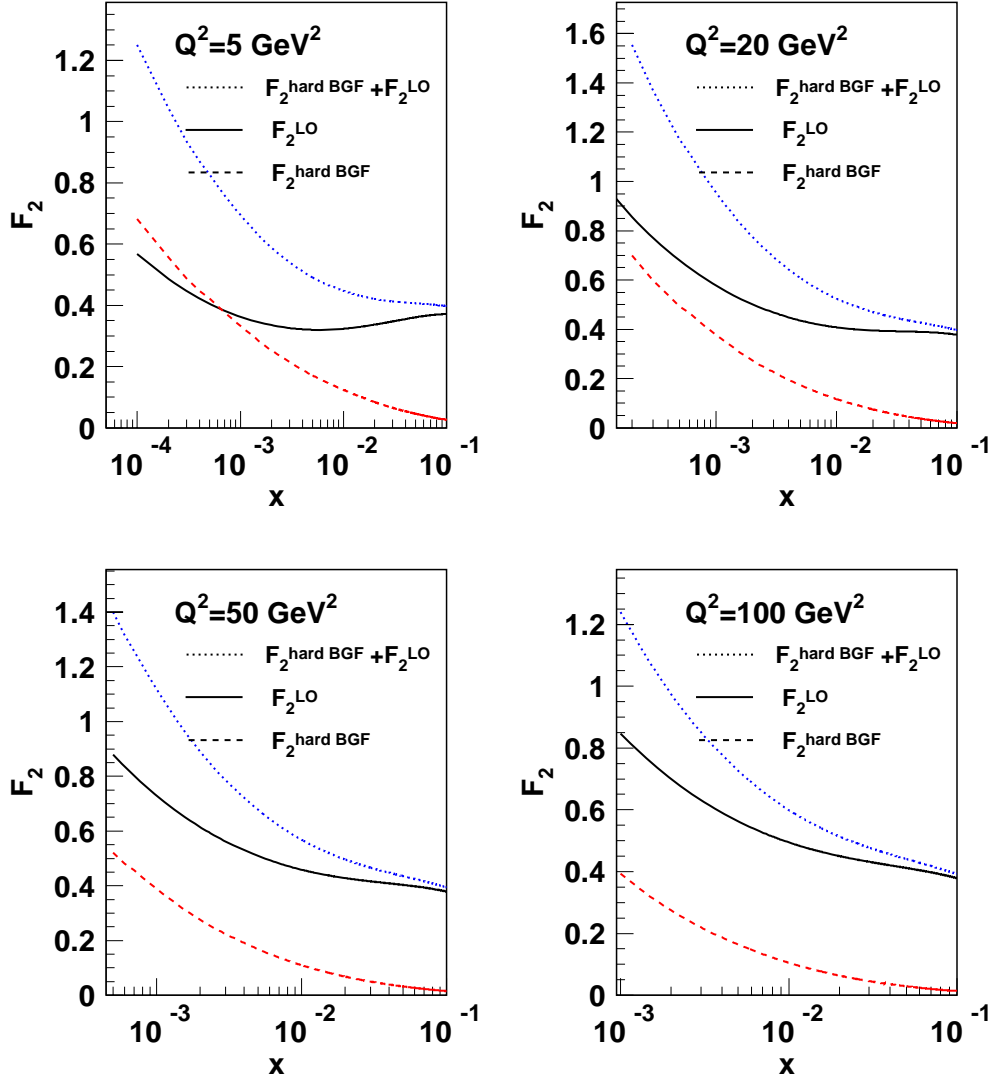


Figure 5.9: F_2^{LO} and $F_2^{\text{BGF hard}}$ and the sum of both for Q^2 values of 5, 20, 50 and 100 GeV^2 .

$F_2^{\text{BGF hard}}$. This is just a consequence of the decreasing available phase space for the LO contribution with decreasing Q^2 . A particular motivation for the treatment of the BGF process in the subtraction method is to describe properly diffractive DIS processes, since in diffractive scattering the gluon dominates the quark scattering. This is demonstrate in fig. (5.10), where we plot the LO contribution as well as the hard contribution of BGF in diffraction. In order to compute the LO contribution in diffraction, we have to calculate the diffractive parton densities in the BS-scheme. This can be simply done

by replacing the parton densities with the diffractive parton densities in eq. (5.25)⁹.

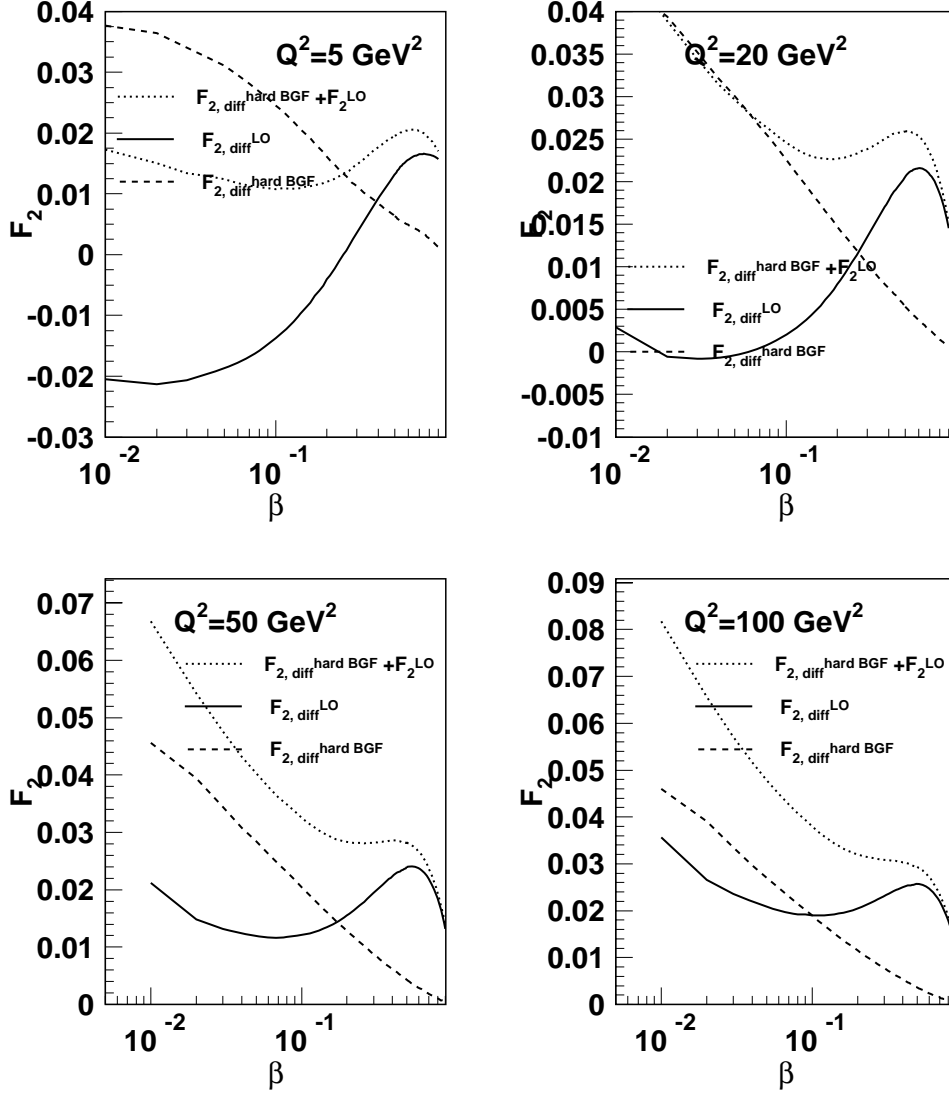


Figure 5.10: $F_{2,\text{diff}}^{\text{LO}}$ and $F_{2,\text{diff}}^{\text{hard BGF}}$ in diffraction at Q^2 values of 5, 20, 50 and 100 GeV^2 .

Fig. (5.10) shows that for all Q^2 values the hard contribution due to BGF is the dominant contribution, in diffraction the gluon introduced contributions are no longer small corrections of the leading order contribution, quite contrary to standard DIS events. Noteworthy are the negative leading order contributions at $Q^2 = 5 \text{ GeV}^2$ and $Q^2 = 20 \text{ GeV}^2$. They can be explained by the fact that the diffractive parton densities

⁹The diffractive parton densities given in [20] are regularized in the $\overline{\text{MS}}$ scheme, thus the usage of eq. (5.25) is justified.

given in [20] are 0 for small Q^2 and x -values. In this case it is not reasonable to calculate the connection between the diffractive parton densities by eq. (5.25), for later usage the LO contribution should be set to 0, if the diffractive parton densities in the $\overline{\text{MS}}$ scheme are 0.

Chapter 6

Conclusion

The correct inclusion of next to leading order corrections in the event generation is of big importance at the lepton-proton collider HERA. The implementation of the NLO corrections in an event generator is problematic, as the corresponding matrix elements diverge in the collinear regions. The standard method to avoid this divergences is to introduce a minimal transverse momentum p_T as cut parameter. This method is inconsistent, it introduces a critical dependency on the p_T -cut itself. In this work, a new regularization scheme, the subtraction scheme, was studied quantitatively for the first time. It allows a consistent inclusion of the NLO contribution due to BGF processes.

The subtraction scheme uses the virtuality of the intermediate quark in a BGF process as a dynamic cut parameter. It allows a *consistent* inclusion of the NLO corrections, as the total structure function derived in this scheme is independent from the specific form of the cut-off function being chosen, a change in the cut-off functions changes the LO as well as the NLO contribution. We calculated the LO contribution and the contribution of BGF processes to the cross section for DIS and diffraction. It could be seen that the subtraction method describes very well the expected behaviour: In DIS the contribution of BGF processes to the cross section increases with decreasing x , but remains generally smaller than the LO contribution, whereas in diffraction the contribution due to BGF events dominates the total cross section.

The next step should be the implementation of the existing programs in the event generator RAPGAP [9]. This should be straightforward, since event generation in the subtraction scheme and in the existing Monte Carlo RAPGAP is based on the same algorithm. This should allow for the first time to study the hadronic final state in diffraction avoiding the critical cut at high p_T -values.

From the theoretical viewpoint it would be interesting to include the contribution of QCDC processes and virtual corrections in the subtraction scheme.

Appendix A

Integration methods

A.1 Linear integration method

In order to create an interface between the integration routines and the different integrands we can simply change the boundaries of the integrals of the type

$$\int_a^1 f(x) dx, \tag{A.1}$$

where a can be an arbitrary function of x , to an integral of the form

$$\int_0^1 g(y) dy. \tag{A.2}$$

This can be obtained by the substitution

$$y = \frac{x - a}{1 - a} \Rightarrow dx = dy (1 - a). \tag{A.3}$$

It follows that

$$\int_a^1 f(x) dx = \int_0^1 f(x)(1 - a) dy = \int_0^1 g(y) dy \tag{A.4}$$

where

$$g(y) = (1 - a)f(x). \tag{A.5}$$

A.2 Importance sampling method

A common situation is the one in which the integrand function $f(x)$ is non-negative in the allowed x range $x_{min} \leq x \leq x_{max}$: $f(x)$ could be a differential cross section, a fragmentation function, etc. We now want to find a transformation of the function $f(x)$ such that the number of x -values taken by the integration routine in order to calculate the root $F(x)$ is proportional to $f(x)$. For example, if the function has a local maximum or a singularity for some value \bar{x} , then the integration routine performs a higher number of samplings near to \bar{x} than far away from it.

If it is possible to find a root function $F(x)$, which has a known inverse function $F^{-1}(x)$, x can be calculated by

$$\int_{x_{min}}^x f(x)dx = R \int_{x_{min}}^{x_{max}} f(x) dx \Rightarrow x = F^{-1}[F(x_{min}) + R(F(x_{max}) - F(x_{min}))]. \quad (\text{A.6})$$

In the first term we ask a fraction R of the total area under $f(x)$ to be on the left of $f(x)$ [13]. Unfortunately the functions which we want to integrate are rarely so well behaved that it is possible to find the function $F(x)$ with its known inverse function. Therefore we have to find a more sophisticated way to compute a number of samplings proportional to the value of the integrand $f(x)$. Let us now assume that the function $f(x)$ can be approximated by a function $g(x)$ which can be integrated analytically, thus having a known root and inverse function. We could calculate the x -samplings using the simpler function $g(x)$ and the method explained in eq. (A.6). The integral of $f(x)$ is then given by

$$I = \int f(x)dx = \int \frac{f(x)}{g(x)}g(x)dx \simeq \sum_i \frac{f(x_i)}{g(x_i)} \int g(x)dx. \quad (\text{A.7})$$

Because of the choice $f(x) \sim g(x)$, the ratio $f(x)/g(x)$ is more or less constant and independent of x . In the following sections we will show two examples to clarify the application of this integration method to our cases.

A.2.1 Example #1: $g(x) = \frac{1}{x}$

As a first example, we assume that the function $f(x)$ can be approximated by the analytically integrable function $g(x) = 1/x$, with the root $G(x) = \log x$ and the inverse function $G^{-1}(x) = \exp(x)$. With eq. (A.6) we then find

$$x = x_{min} \left(\frac{x_{max}}{x_{min}} \right)^R. \quad (\text{A.8})$$

Solving eq. (A.8) for R we obtain

$$R = \frac{\log x - \log x_{min}}{\log x_{max} - \log x_{min}} \quad (\text{A.9})$$

Using eq. (A.7) the integral is then given by

$$\int f(x)dx \simeq \sum_i x_i f(x_i) \int_{x_{min}}^{x_{max}} g(x)dx = \sum_i x_i f(x_i) \log \frac{x_{max}}{x_{min}} \quad (\text{A.10})$$

In the calculation of σ_{BGF} the eqs. (3.31), (5.9) and (3.36) as well as the shower contribution of eq. (5.2) are all proportional to $1/\xi$. In order to get a stable result of the the integrands can be approximated by $g(\xi) = 1/\xi$ and this example can be applied.

A.2.2 Example #2: $f(x) = \frac{a}{1+x} + \frac{b}{1-x}$

A more complicated function $f(x) = \frac{a}{1+x} + \frac{b}{1-x}$ can be approximated by a function $g(x) = \frac{1}{1-x^2}$. The root of $g(x)$ is $G(x) = \text{arctanh}(x)$, and its inverse function $G^{-1}(x) = \tanh(x)$. If $x_{max} = -x_{min}$ from eq. (A.6) we obtain

$$x = \frac{-x_{max} + \tanh(2R \text{arctanh}(x_{max}))}{1 - x_{max} \tanh(2R \text{arctanh}(x_{max}))}. \quad (\text{A.11})$$

It follows

$$R = \frac{\text{arctanh}\left(\frac{x+x_{max}}{1+x x_{max}}\right)}{2 \text{arctanh}(x_{max})}. \quad (\text{A.12})$$

The integral is then given by

$$\begin{aligned} \int f(x) dx &\simeq \sum_i (1-x_i)^2 f(x_i) \int_{-x_{max}}^{x_{max}} g(x) dx \\ &= \sum_i (1-x_i)^2 f(x_i) 2 \text{arctanh}(x_{max}). \end{aligned} \quad (\text{A.13})$$

This example is used to transform the integration in the unsubtracted cross section of eq. (5.9) as well as the shower contribution of eq. (5.8). In these special cases we have to deal with integrands of the form

$$f(\cos \theta) = \frac{a}{1 + \cos \theta} + \frac{b}{1 - \cos \theta} \quad (\text{A.14})$$

and $\cos(\theta_{max}) = -\cos(\theta_{min})$, In order to avoid divergences of the integrands of eqs. (5.9) and eq. (5.8) we have chosen in this work $\cos(\theta_{max}) = 0.999999$.

A.3 Calculation of F_2^{charm}

A.3.1 Results of the numeric integration

In order to calculate the cross section due to BGF processes for charm quarks as discussed in Chapter 2, several integration routines were used to perform the integration over the variable ξ : *DGAUSS* and *RADAPT* from the CERNLIB [21] together with *GADAP* and *DGAUSSKEPS* from [9]. The result of these numeric integrations are shown in fig. (A.3.1): big discrepancies between the routines *DGAUSS* and *DGAUSSKEPS* and between *GADAP* and *RADAPT* can be seen. Furthermore the F_2^{charm} curve calculated by all integration routines shows discontinuities.

Both observations gives us a strong hint that the integrand contains local maxima making the numeric integration very unstable. In order to verify this assumption we plot in fig. (A.3.1) the integrand of eq. (3.36) with a simplified gluon density $g(\xi) = 3(1-\xi)^5/\xi$: the integrand shows a maximum for $\xi \sim 0.15$. This can bring the numerical integration routines into difficulties, as these programs usually calculate the integral only for few ξ -values. If the integrand shows big fluctuations in relatively small ranges of ξ , we obtain only a very poor estimation of the integral.

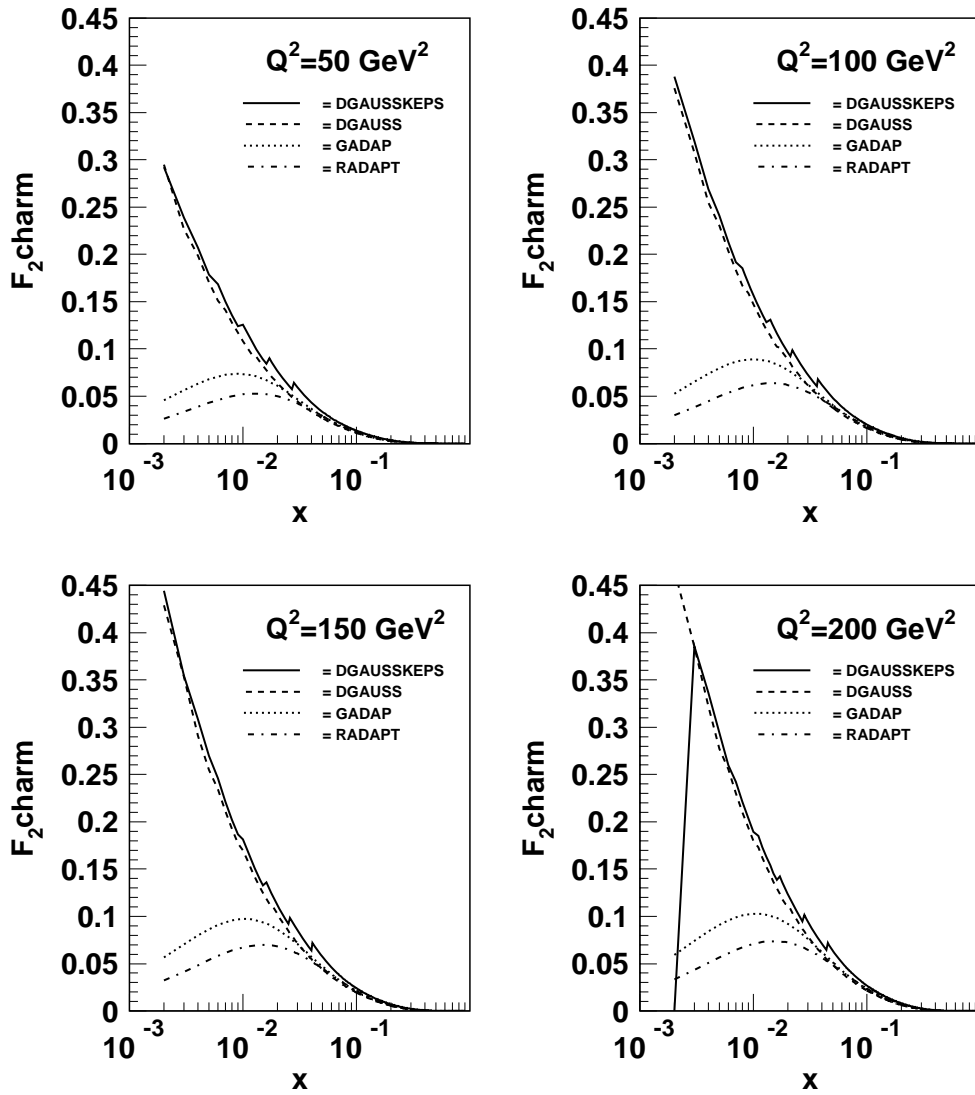


Figure A.1: Computation of F_2^{charm} with the integration routines DGAUSS, DGAUSSKEPS, GADAP and RADAPT without any transformation.

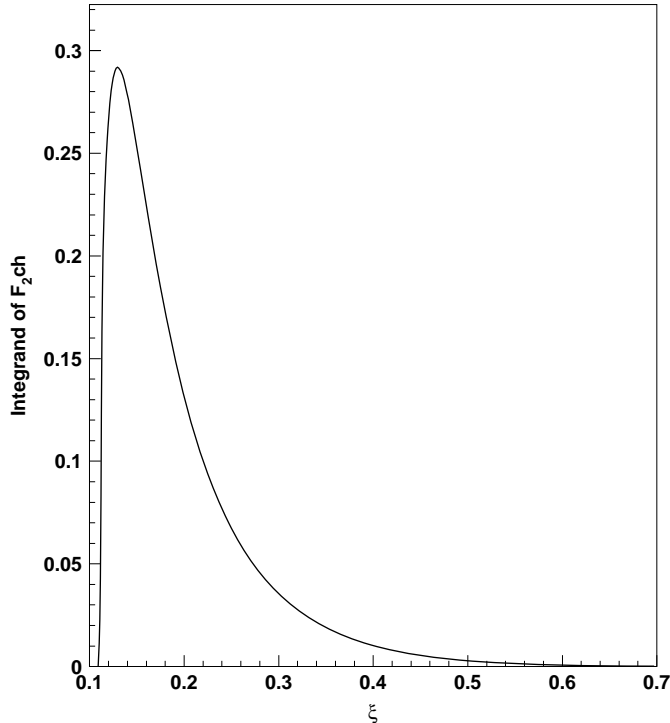


Figure A.2: *Integrand of eq. (3.36) with a simplified gluon density.*

A.3.2 F_2^{charm} with the importance sampling method

In section (A.2) we have introduced a transformation method which ensures that the number of ξ -values taken by the different integration routine are proportional to the value of the integrand. This guaranties that in proximity of a maximum the integration routines take a bigger number of ξ -samples to compute the integral. As done in the example in (A.2) we can approximate the integrand of eq. (3.36) by a simpler function, i.e. $g(\xi) = 1/\xi$. From eqs. (A.10) and (3.36) it follows that

$$\begin{aligned}
 F_2^{\text{charm}, BGF}(x, Q^2, m_c^2) &= \frac{1}{2\pi} e_q^2 \alpha_s(\mu^2) \int_{ax}^1 C^{\text{charm}} z f_g(\xi, \mu^2) d\xi \\
 &= \int_{ax}^1 f(\xi) d\xi \simeq \sum_i f(\xi_i) \xi_i \log \frac{1}{ax}. \quad (\text{A.15})
 \end{aligned}$$

Using this trick, usually called *logarithmic transformation*, the integrand of eq. (3.36) becomes smoother, since it is multiplied with a weighting factor $\xi_i \log \frac{1}{ax}$.

In figure A.3 we finally show F_2^{charm} calculated with the different routines, always using eq. (A.15). Using the logarithmic transformation we obtain a continuous curve for $F_2^{\text{charm}, BGF}$ and reduced discrepancies between the different integration routines. Further investigations showed that using the integration routine *GADAP* we obtain

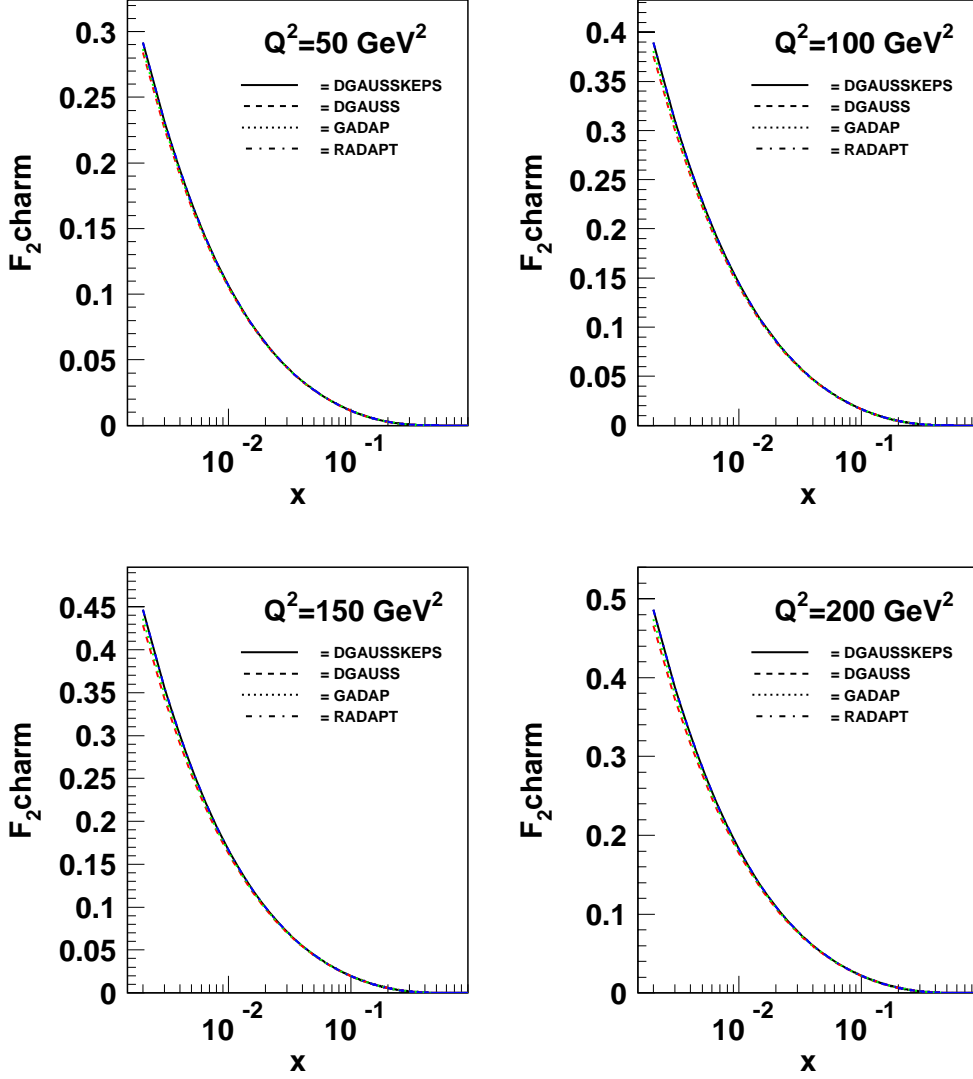


Figure A.3: $F_2^{\text{charm BGF}}$ integrated with the logarithmic transformation.

results which are competitive with a direct numeric integration of eq. (3.36) and an integration using the importance sampling transformation method. Moreover the result of the integration routine did only slightly change as a function of the required precision.

Appendix B

Regularization of BGF in the Massive–Gluon scheme

The Massive–Gluon (MG) scheme offers the possibility to treat the order α_s corrections for BGF in a consistent manner: the divergences in the BGF matrix element can be regulated by taking the incoming gluon slightly off-shell and space like, $g^2 = -m_g^2$ [7]. In this case for the differential cross section is given by

$$\frac{d\hat{\sigma}_\Sigma^g}{d\hat{t}} = \pi^2 e_q^2 \frac{z^2}{Q^4} \alpha \alpha_s \left[\frac{\hat{u}}{\hat{t}} + \frac{\hat{t}}{\hat{u}} - 2 \frac{\hat{s} Q^2}{\hat{u} \hat{t}} + 2 m_g^2 \frac{(\hat{t} + \hat{u} + m_g^2)}{\hat{t} \hat{u}} - Q^2 m_g^2 \left(\frac{1}{\hat{u}^2} + \frac{1}{\hat{t}^2} + \frac{4}{\hat{u} \hat{t}} \right) \right], \quad (\text{B.1})$$

where z is defined in eq.(3.3) and g indicates that MG is the chosen regulating scheme. The subscript Σ indicates that we have summed over all virtual photon polarization states by the replacement

$$\sum_\lambda \epsilon_\mu \epsilon_\nu^*(\lambda) \rightarrow -g_{\mu\nu}. \quad (\text{B.2})$$

This differential cross section is a combination of the transverse and longitudinal differential cross sections. For the total cross section holds

$$\sigma_\Sigma = 2\sigma_T - \sigma_L. \quad (\text{B.3})$$

Without the gluon mass the integration limits for the partonic cross section were

$$\hat{t}_0 = -(\hat{s} + Q^2) = -Q^2/z, \quad \hat{t}_1 = 0 \quad (\text{B.4})$$

leading to divergences for $t = 0$. By introducing the gluon mass we obtain new integration limits:

$$\hat{t}_0 = \hat{u}_{max} = -(\hat{s} + Q^2) = -Q^2/z, \quad (\text{B.5})$$

$$\hat{t}_1 = \hat{u}_{min} = -m_g^2 z. \quad (\text{B.6})$$

Integrating eq. (B.1) over \hat{t} we obtain

$$\hat{\sigma}_{MG, \Sigma}^g = \pi^2 e_q^2 \frac{z^2}{Q^4} \alpha \alpha_s 2 \left(z^2 + (1-z)^2 \log \frac{Q^2}{z^2 m_g^2} - 2 \right). \quad (\text{B.7})$$

The differential cross section for the scattering of longitudinal photons is (see [7])

$$\frac{d\hat{\sigma}_L^g}{d\hat{t}} = \pi\alpha\alpha_s e_q^2 \frac{z}{Q^2} \frac{4z^2}{Q^2} 2(1-z). \quad (\text{B.8})$$

Equation (B.8) contains no divergent terms and can easily be integrated over \hat{t} , giving

$$\hat{\sigma}_L^g = \pi\alpha\alpha_s e_q^2 \frac{4z^2}{Q^2} 2(1-z). \quad (\text{B.9})$$

The partonic cross sections in eqs. (B.8) and (B.7) have to be weighted with the gluon density $f_g(\xi)$ and then be integrated over ξ to get the total cross sections

$$\sigma_\Sigma(\gamma^*N) = \int_x^1 \hat{\sigma}_\Sigma f_g(\xi) d\xi \quad (\text{B.10})$$

$$\sigma_L(\gamma^*N) = \int_x^1 \hat{\sigma}_L f_g(\xi) d\xi. \quad (\text{B.11})$$

where σ_Σ and σ_L are connected to σ_T by eq. (B.3). With (3.31 and (3.33) we finally get for the gluon contribution to F_2

$$F_2^g(x, Q^2) = 2xe_q^2 \int_x^1 \frac{d\xi}{\xi} f_g(\xi) \left(\frac{\alpha_s}{2\pi} P_{g \rightarrow q\bar{q}}(z) \log \frac{Q^2}{m_g^2} + \alpha_s f_{MG}^{g,DIS}(z) \right) \quad (\text{B.12})$$

where:

- $f_g(\xi)$ is the probability to find a gluon with momentum $g = \xi P$, where P is the proton four momentum;
- the term

$$P_{g \rightarrow q\bar{q}}(z) = \frac{1}{2}(z^2 + (1-z)^2) \quad (\text{B.13})$$

is one of the so called Altarelli – Parisi splitting functions. It indicates the probability that a gluon annihilates into a quark – antiquark pair is such that the quarks have a fraction z of the gluon's momentum. The splitting functions are independent of the chosen regularization scheme .

- The expansion of the last term is

$$\alpha_s f_{MG}^{g,DIS}(z) = \alpha_s [-(z^2 + (1-z)^2) \log(z) - 1 + 3z - 3z^2]. \quad (\text{B.14})$$

This last is scheme dependent, it is usually called *little f function*.

In the MG scheme F_2^g splits into two terms representing two different kinematical regions

$$F_2^g(x, Q^2) = F_2^{g, shower} + F_2^{g, hard} \quad (\text{B.15})$$

where

$$F_2^{g, shower} = 2xe_q^2 \int_x^1 \frac{d\xi}{\xi} f_g(\xi) \frac{\alpha_s}{2\pi} P_{g \rightarrow q\bar{q}}(z) \log \frac{Q^2}{m_g^2} \quad (\text{B.16})$$

represents that part of F_2^g arising from processes with

$$Q^2 > Q_1^2 > m_g^2, \quad (\text{B.17})$$

where Q_1^2 is the virtuality of the intermediate quark in BGF processes . The second term in eq. (B.15)

$$F_2^{g,hard} = 2xe_q^2 \int_x^1 \frac{d\xi}{\xi} f_g(\xi) \alpha_s f_{MG}^{g,DIS}(z) \quad (\text{B.18})$$

represents the contribution to F_2^g due to processes which satisfy the condition

$$m_g^2 > Q^2. \quad (\text{B.19})$$

Despite the dynamic cut parameter Q_1^2 in the subtraction scheme, we have a fixed cut parameter m_g in the Massive Gluon scheme.

List of Figures

2.1	e - p -scattering	3
2.2	BGF and QCDC	6
3.1	Parton splitting	10
3.2	Boson – Gluon Fusion	11
3.3	Measured and calculated F_2^{charm}	16
3.4	QCD –Compton scattering	17
3.5	The NLO contribution of light quarks to the structure function	19
4.1	Spacelike shower evolution	23
4.2	Four momenta in boson-gluon fusion	26
5.1	Differential cross section of BGF	32
5.2	Quark and antiquark term in BGF	33
5.3	Differential cross section due to the shower algorithm	34
5.4	Differential cross section due to the shower algorithm	36
5.5	The hard contribution of BGF	37
5.6	F_2^{BGF} derived by the subtraction method	39
5.7	The structure function in diffractive processes	40
5.8	The LO contribution to F_2 in the \overline{MS} scheme and the BS scheme	43
5.9	F_2^{LO} and $F_2^{BGF\ hard}$	44
5.10	$F_{2,diff}^{LO}$ and $F_{2,diff}^{hard\ BGF}$	45
A.1	F_2^{charm}	52
A.2	Integrand of F_2^{charm}	53
A.3	$F_2^{charm\ BGF}$ integrated with the logarithmic transformation	54

References

- [1] C.Friberg, T. Sjöstrand, Some thoughts on how to match Leading Log Parton Showers with NLO Matrix elements, 1999, hep-ph-9906316.
- [2] J.Collins, Subtraction method for NLO corrections in Monte-Carlo event generators for leptonproduction, 2000, hep-ph/0001040.
- [3] R. Ellis, *QCD and Collider Physics* (Cambridge University Press, 1996).
- [4] F. Halzen, A. Martin, *Quarks and Leptons* (J. Wiley & Sons, Inc., 1984).
- [5] R. Peccei, R. Rückl, *Nucl. Phys.* **B 162** (1980) 125.
- [6] Particle Data Group; L. Montanet et al., *Phys. Rev.* **D 50** (1994).
- [7] R.D.Field, *Applications of Perturbative QCD* (Addison-Wesley Publishing Company, 1989).
- [8] M. Glück, E. Reya, A. Vogt, *Z. Phys.* **C 67** (1995) 433.
- [9] H. Jung, *The RAPGAP Monte Carlo for Deep Inelastic Scattering, version 2.08*, Lund University, 1999, <http://www-h1.desy.de/~jung/rapgap.html>.
- [10] ZEUS Collaboration; J. Breitweg et al., *Eur. Phys. J.* **C 6** (1999) 67.
- [11] M. Glück, E. Reya, A. Vogt, *Z. Phys.* **C 53** (1992) 127.
- [12] H. Plochow-Besch, PDFLIB Version 7.09, User's Manual. W5051 1997.07.02 CERN-PPE, 1997.
- [13] T. Sjöstrand, *PYTHIA 5.7 and JETSET 7.4 - Physics and manual*, 1993, cERN-TH.7112/93.
- [14] M. Bengtsson, T. Sjöstrand, *Z. Phys.* **C 37** (1988) 465.
- [15] G. Altarelli, G. Parisi, *Nucl. Phys.* **B 126** (1977) 298.
- [16] T. Sjöstrand, *Phys. Lett.* **B 157** (1985) 321.
- [17] T. Sjöstrand, *Comp. Phys. Comm.* **82** (1994) 74.
- [18] H. Jung, *The RAPGAP Monte Carlo for Deep Inelastic Scattering, version 2.08*, Lund University, 1999, <http://www-h1.desy.de/~jung/rapgap.html>.
- [19] H. Jung, Monte Carlo Implementations of Diffraction at HERA, in *Proc. of the LISHEP workshop on diffractive physics*, edited by A. Santoro (Rio de Janeiro, Brazil, Feb 16 - 20, 1998).
- [20] H1 Collaboration; C. Adloff et al., *Z. Phys.* **C 76** (1997) 613.
- [21] *CERNLIB*, CERN, 2000, <http://wwwinfo.cern.ch/asd/cernlib/libraries.html>.

Acknowledgements

Many people helped me along the way to write this thesis. Here I want to acknowledge specific contributions from a number of persons. Most of all I wish to thank Hannes Jung for the excellent and supportive supervision during the past year, he called my attention to the interesting topics of this thesis. Inspiring and motivating discussions let me learn a lot about the underlying physics problems. Furthermore I want to thank Peter Schleper for the admission to the H1-working group at the physical institute of the university of Heidelberg and his useful comments and helpful suggestions on this thesis. I am grateful to Jürgen von Krogh for being the second expert evaluating this thesis. I wish to thank John Collins for the fruitful discussions on the subtraction method. Special thanks to Vincenzo Chiochia for proof-reading this thesis and his helpful remarks on my “German English”. His support and friendship was fundamental for the completion of this work. Finally I want to thank all the Ph.D. students and postdocs at DESY and the Physical Institute of the University of Heidelberg, who helped me with this thesis, above all Nicola Coppola, Birger Koblitz, Christiane Risler and Thomas Hadig.

Ich versichere, daß ich diese Arbeit selbständig verfaßt und keine anderen als die angegebenen Quellen und Hilfsmittel benutzt habe.

Heidelberg, den

.....
Sabine Helge Hiltrud Schilling